Scientific Reports

https://doi.org/10.1038/s41598-026-38867-z

Article in Press

RHA/TiO_2-[bip]-$NH_2^+NO_3^-$ as an efficient catalyst for the solvent-free synthesis of 1,8-dioxo-decahydroacridine and 2,3-dihydroquinazolin-4(1*H*)-one derivatives

Received: 7 December 2025

Accepted: 31 January 2026

Published online: 10 February 2026

Cite this article as: Aloueian F., Shirini F., Gholinejad M. *et al.* RHA/TiO_2-[bip]-$NH_2^+NO_3^-$ as an efficient catalyst for the solvent-free synthesis of 1,8-dioxo-decahydroacridine and 2,3-dihydroquinazolin-4(1*H*)-one derivatives. *Sci Rep* (2026). https://doi.org/10.1038/s41598-026-38867-z

Fatemeh Aloueian, Farhad Shirini, Mohammad Gholinejad & José M. Sansano

RHA/TiO_2-[bip]-$NH_2^+NO_3^-$ as an efficient catalyst for the solvent-free synthesis of 1,8-dioxo-decahydroacridine and 2,3-dihydroquinazolin-4(1*H*)-one derivatives

Fatemeh Aloueian[a], *Farhad Shirini*[b*], *Mohammad Gholinejad* [a], *José M. Sansano*[c]

[a] Department of Chemistry, Institute for Advanced Studies in Basic Sciences (IASBS), Zanjan 45137-66731, Iran

[b] Department of Organic Chemistry, Faculty of Chemistry, University of Guilan, Rasht, 41335 19141, Iran. E-mail: shirini@guilan.ac.ir

[c] Departamento de Química Orgánica, Instituto de Síntesis Orgánica, and Centro de Innovación en Química Avanzada (ORFEO-CINQA), Universidad de Alicante, 03690 Alicante, Spain

Abstract

In this study, a novel heterogeneous catalyst with the selected formula of RHA/TiO_2-[bip]-$NH_2^+NO_3^-$ was successfully synthesized and characterized, using of various techniques, including FT-IR, ^1H NMR, ^{13}C NMR, TEM, XRD, XPS, TGA, EDX, and SEM mapping. The catalytic performance of this material was then evaluated in the synthesis of 1,8-dioxo-decahydroacridine and 2,3-dihydroquinazolin-4(1*H*)-one derivatives. The products were formed in very short reaction times under solvent-free conditions with excellent yields. In addition, the reusability of the catalyst was investigated, confirming its stability for at least five consecutive runs and also its ability to use in green and sustainable synthetic processes.

Introduction

Multi-component reactions (MCR) are an effective and novel strategy towards the construction of organic compounds by the assembly of three or more reactants simultaneously in a one-pot step. The reaction permits the construction of compounds that embody the essential building blocks of the reactants. MCRs are also aligned with principles of green chemistry due to their higher efficiency, favorable atom economy, minimization of the steps of the reactions and number of the intermediates, as well as minimizing solvent consumption with conservation of time and energy, and minimization of unwanted wastes. Moreover, the potential of the procedure to implement simultaneously the construction of carbon–carbon as well as carbon–heteroatom linkages within an integrated step has made the procedure an effective tool towards the assembly of rapidly complex and bioactive compounds. Use of no solvent in some of these types of reactions can also bring higher efficiency as well as stability to the procedure [1–7].

Nitrogen heterocycles are of paramount importance for organic chemistry and pharmacology by virtue of their structural diversity and extremely wide range of biological activity. Derivatives of such compounds are employed globally for synthesizing anticancer, anti-inflammatory, antibacterial, and antiviral medicines. These compounds are very important in agriculture and materials science [8–12]. The importance of these compounds be more clear when we notice that more than 75% of Food and Drug Administration (FDA) approved small-molecule drugs incorporate nitrogen heteroatoms [13]. Based on their considerable characteristics, Synthesis of nitrogen heterocyclic compounds, especially aromatic and polycyclic variants, has therefore been at the core of the scientific enterprise over the past decades.

Among the nitrogen-containing heterocycles, 1,8-dioxo-decahydroacridine and 2,3-dihydroquinazolin-4(1*H*)-one derivatives hold significant importance in the fields of organic and medicinal chemistry due to their extensive range of biological activities. The synthesis of 1,8-dioxo-decahydroacridine is typically achieved through the Hansch reaction, an efficient multi-component reaction involving an aldehyde, a β-ketoester, and a nitrogen source, facilitating the production of various derivatives with therapeutic applications such as vasodilators, bronchodilators, antiplatelet agents, and chemosensitizers[14–17]. Similarly, 2,3-dihydroquinazolin-4(1*H*)-ones, as valuable bicyclic heterocycles, are usually synthesized by the ternary reaction of isatoic anhydride, ammonium acetate, and an aldehyde, affording extensive pharmacological properties such as antitumor, antibacterial, antifungal, antihypertensive, and antioxidant activities[18–22].

In recent years, the use of environmentally friendly catalysts, especially acidic ionic liquids (ILs), has been recognized as a suitable substitute for conventional inorganic acid catalysts due to such virtues as thermal stability, negligible vapor pressure, nonflammability, and structural designability of these [23,24]. These compounds, which are composed of various anions and are liquid at temperatures below 100 °C, can act as solvents and also catalysts [25,26]. However, challenges such as high viscosity, high consumption, difficulty in recovery, and limited stability in the presence of air and moisture have limited their application, especially at an industrial scale [27,28]. One effective solution to overcome these limitations is the immobilization of ionic liquids on natural or synthetic solid supports, which, while maintaining the advantages of ILs, allows the preparation of heterogeneous catalysts with easy separation, reuse, and reduced catalyst consumption and cost [29–32]. This approach, especially using natural or inorganic solid supports such as rice husk ash (RHA) and metal oxides such as TiO_2, improves the catalytic properties, increases the specific surface area, and facilitates the catalyst recyclability [33,34]. RHA, which can be obtained from the combustion of rice husk, is a high surface natural substrate that has varying immobilisation capabilities of ionic liquids [35,36]. TiO_2 nanoparticles are another suitable

substrate for this purpose because of their low cost, ease of synthesis, and favorable thermal stability [37]. Merging such substrates with ionic liquids resulted in the synthesis of nanocatalysts that improve high mechanical stability, reusability, and remarkable efficiency in multicomponent organic reactions. Moreover, Traditional homogeneous Brønsted acids, including H_2SO_4 and p-toluenesulfonic acid, are widely used in condensation and multicomponent reactions; however, their strong acidity often leads to corrosive reaction conditions, limited selectivity, and difficulties in catalyst recovery. In contrast, acidic ionic liquids provide Brønsted acidic sites with comparatively milder acidity, which is sufficient to promote proton-assisted transformations while minimizing side reactions and improving selectivity [38,39].

Because of the above mentioned subjects, in this study we have investigated the preparation and application of a novel nanocatalyst based on TiO_2 and RHA which is formulated a RHA/TiO_2-[bip]-$NH_2^+NO_3^-$, efficient in the synthesis of 1,8-dioxo-decahydro acridine and 2,3-dihydroquinazolin-4(1*H*)-one derivatives.

Experimental

Materials and methods

All chemicals were used as received, without further purification. The RHA sample was prepared according to the procedures described in the literature [40]. ^{1}H NMR and ^{13}C NMR spectra were recorded at 400 MHz and 100 MHz, respectively, on a Bruker Avance HD apparatus in DMSO-d_6 (Bruker, Germany). The Fourier-transform infrared spectra (FT-IR) were recorded with a VERTEX 70 (Brucker, Germany). The crystallographic studies were carried out using an X-ray diffractometer (Bruker D8 Advance, Bruker AXS GmbH, Karlsruhe, Germany) equipped with Cu Kα radiation (λ = 1.5406 Å). The physical morphologies were investigated by transmission electron microscopy (TEM, JEOL JEM-2010, JEOL Ltd., Tokyo, Japan) and field emission scanning electron microscopy (FE-SEM,

JEOL JSM-840, JEOL Ltd., Tokyo, Japan). X-ray photoelectron spectroscopy (XPS) measurements were carried out using a VG Microtech Multilab 3000 spectrometer (VG Microtech Ltd., East Grinstead, UK) equipped with an Al Kα anode .The elemental mapping was performed using a scanning electron microscope (SEM, Hitachi S-3000N, Hitachi High-Technologies Corporation, Tokyo, Japan).

Preparation of nanoporous RHA/TiO_2

Rice husk ash (1.0 g) was suspended in absolute ethanol (6 mL) and stirred at room temperature for 30 minutes. Titanium tetraisopropoxide (TTIP) was then dropped into this suspension under continuous stirring for 2 hours with a TTIP-to-ethanol volume ratio of 1:4. Deionized water (16 mL) was further added to the solution stepwise, following a TTIP-to-water ratio of 1:10, and stirring was maintained further for 2 hours to complete the hydrolysis of all TTIP. The product material was separated through filtration, washed with water, and dried in an oven temperature of 80 °C. Last of all, the solid so prepared was calcined at a temperature of 500 °C for 3 hours to prepare the RHA/TiO_2 nanocomposite.

Preparation of RHA/TiO_2-[bip]-NH_2^+ NO_3^-

To a suspension of 5 g of RHA/TiO_2 in 25 mL of ethanol, bis-3-(trimethoxysilylpropyl)-amine (5 mmol) was added, and the resulting suspension was stirred under reflux conditions for 3 days. It was filtered to room temperature upon precipitation collection and washed subsequently with 10 mL of diethyl ether (Et_2O) and vacuum dried. The reaction product (6.5 g) so prepared was suspended in 20 mL of anhydrous CH_2Cl_2. While vigorously stirring in an ice bath maintained at 0 °C, 5 mmol of concentrated HNO_3 (60%) was added dropwise. The mixture was then refluxed with stirring for 24 hours. After filtration, RHA/TiO_2-[bip]-NH_2^+ NO_3^- was obtained as a white solid (Fig. 1).

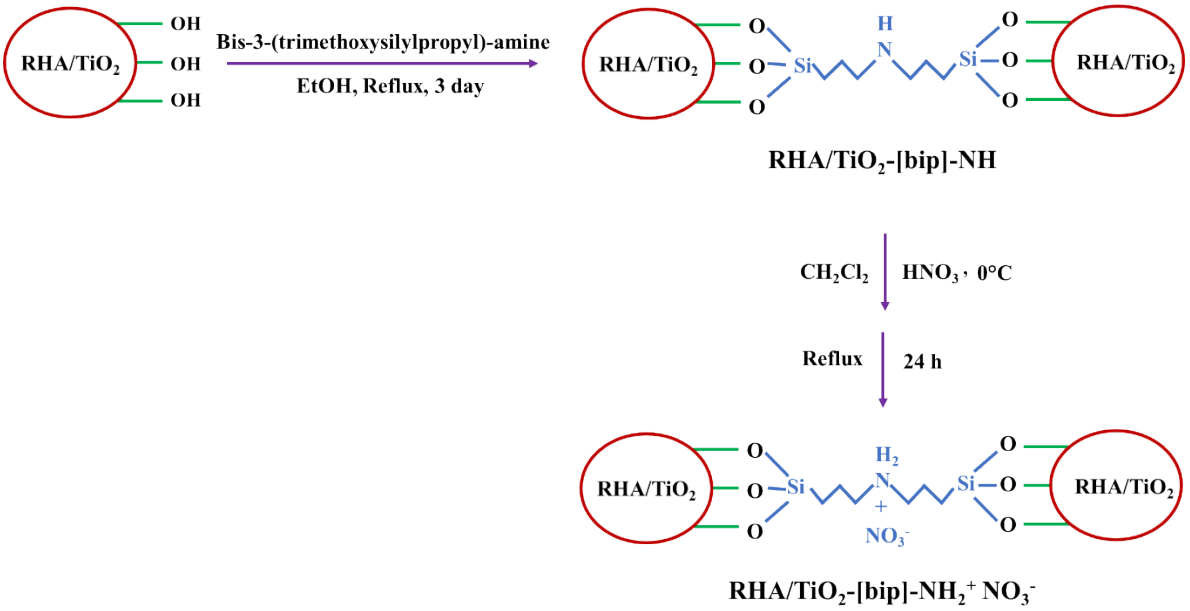

Fig. 1. Preparation of RHA/TiO_2-[bip]-NH_2^+ NO_3^-.

General procedure for the synthesis of 2,3-dihydroquinazolin-4(1*H*)-ones

A mixture of isatoic anhydride (1 mmol), aromatic aldehyde (1 mmol), ammonium acetate (1.2 mmol), and the catalyst (20 mg) was stirred under solvent-free conditions at 100 °C. TLC analysis by thin-layer chromatography (TLC) in *n*-hexane/EtOAc (7:3, *v/v*) as eluent indicated the progress of the reaction. After its completion, it was treated with hot ethanol (10 mL) and filtered to separate the catalyst through its insolubility. The end product so formed was purified through chromatography by column and/or plate to give the requested pure 2,3-dihydroquinazolin-4(1*H*)-one derivatives.

General procedure for the synthesis of 1,8-dioxo-decahydroacridines

A mixture of dimedone or 1,3-cyclohexanedione (2 mmol), ammonium acetate (1.5 mmol), aromatic aldehyde (1 mmol), and RHA/TiO_2-[bip]-NH_2^+ NO_3^- (20 mg) was stirred at 110 °C in the absence of solvent. The reaction progress was monitored by TLC (*n*-hexane/EtOAc,

4:1). After completion, hot ethanol (10 mL) was added; the catalyst was separated by filtration, and the final product was purified using column or plate chromatography.

Result and discussion

Catalyst characterization

The FT-IR spectra of RHA/TiO_2, RHA/TiO_2-[bip]-NH, and RHA/TiO_2-[bip]-NH_2^+ NO_3^- are given in Fig. 2. For RHA/TiO_2, absorption bands at 1096, 797, and 467 cm^{-1} are due to the asymmetric, symmetric, and bending modes of Si-O-Si, respectively. An absorption band appearing at 1671 cm^{-1} corresponds to the vibrational mode of Ti-O-Ti. Furthermore, absorption bands appearing at 3424 and 1633 cm^{-1} are due to the stretching and bending vibrations of Si-OH and/or Ti-OH hydroxyl groups and adsorbed water, respectively. For RHA/TiO_2-[bip]-NH, a peak appearing at 1102 cm^{-1} is due to the C-C-C bending vibration, and a peak appearing at 2928 cm^{-1} is due to the stretching vibration of the C-H group [33,34,41–45]. In the case of the final catalyst, in addition to the other vibrations related to the named functional groups in RHA/TiO_2 and RHA/TiO_2-[bip]-NH, a peak appearing due to the stretching vibration of NO_3^- ions is found to appear at 1384 cm^{-1} [46]. Spectral data confirm the formation of a Brønsted acidic ionic liquid on the RHA/TiO_2 surface. the preserved Si–O–Si and Ti–O–Ti bands indicate that the structural integrity of the support remains intact, which is crucial for catalyst stability.

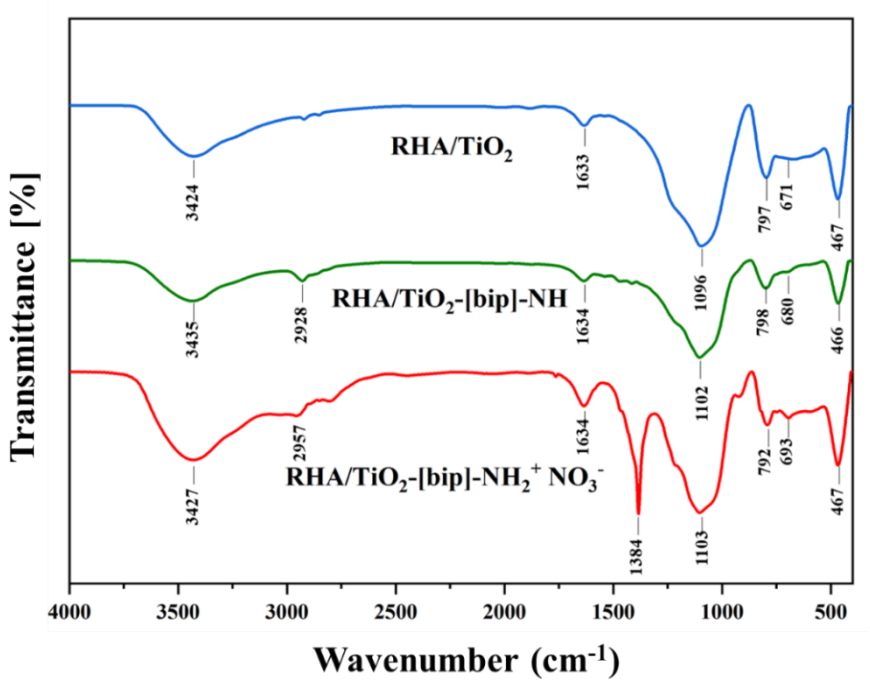

Fig. 2. FT-IR spectra of RHA/TiO_2, RHA/TiO_2-[bip]-NH and RHA/TiO_2-[bip]-NH_2^+ NO_3^-.

The X-ray diffraction (XRD) patterns of RHA/TiO_2, RHA/TiO_2-[bip]-NH, and RHA/TiO_2-[bip]-$NH_2^+NO_3^-$ reveal a broad peak at 2θ = 21.3, which corresponds to the presence of amorphous silica in RHA [33]. The peaks observed at 2θ = 25.3, 37.8, 48.15, 54.2, and 62.5 in the RHA/TiO_2 nanocomposite are associated with the reflections (101), (004), (200), (105), and (211), respectively, indicating that the anatase phase is the sole phase present in all the synthesized materials [45]. The intensities of the peaks for RHA/TiO_2-[bip]-NH and RHA/TiO_2-[bip]-$NH_2^+NO_3^-$ remain largely unchanged compared to the RHA/TiO_2 pattern, suggesting the stabilization of the ionic liquid on the RHA/TiO_2 substrate and that the substrate remains unaltered during the catalyst preparation process. Moreover, the absence of additional crystalline peaks related to the ionic liquid suggests its successful and homogeneous dispersion on the support surface rather than the formation of separate crystalline domains (Fig. 3).

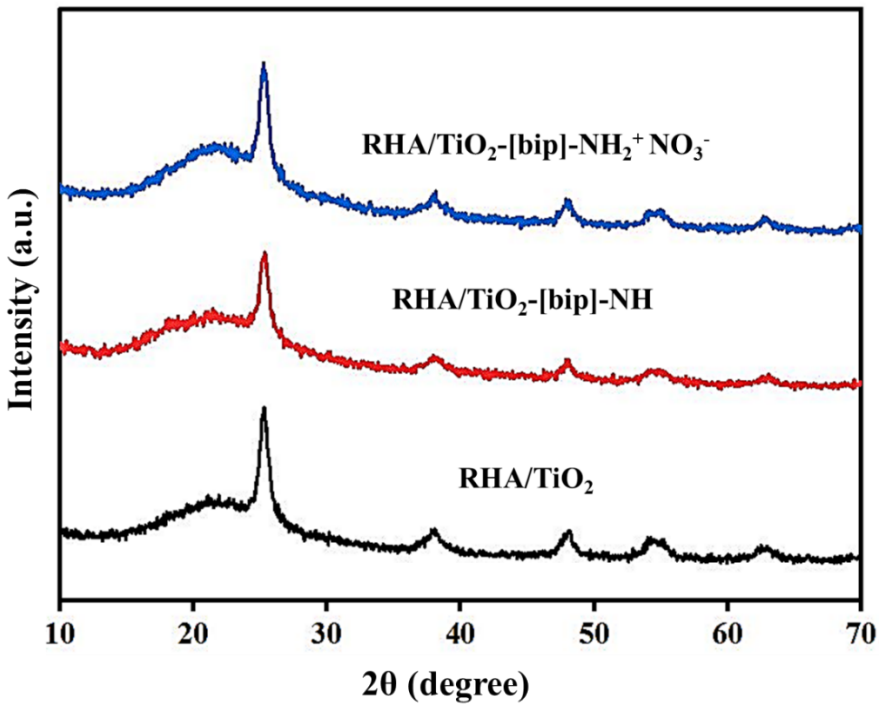

Fig. 3. XRD patterns of RHA/TiO_2, RHA/TiO_2-[bip]-NH and RHA/TiO_2-[bip]-NH_2^+ NO_3^-.

The thermogravimetric analysis (TGA) curves of RHA/TiO_2 and RHA/TiO_2-[bip]-NH_2^+ NO_3^- are presented in Fig. 4. The RHA/TiO_2 sample shows only about 4% weight loss, indicating its high thermal stability. The weight decrease below 100 °C is attributed to the removal of physically adsorbed water, while the gradual loss up to 600 °C can be related to the elimination of terminal groups such as surface -OHs [47]. In contrast, the TGA curve of RHA/TiO_2-[bip]-NH_2^+ NO_3^- exhibits a completely different behavior. The weight below 100 °C corresponds to the release of the adsorbed water. The decreases observed after 100 °C can be ascribed to the thermal decomposition of the ionic parts and complete decomposition of the organic groups attached to the RHA/TiO_2 surface [48]. This enhanced thermal stability can be attributed to strong interactions between the ionic liquid moieties and the solid surface, which restrict molecular mobility and delay thermal degradation. Such improved thermal robustness is particularly advantageous for catalytic applications conducted under elevated temperatures.

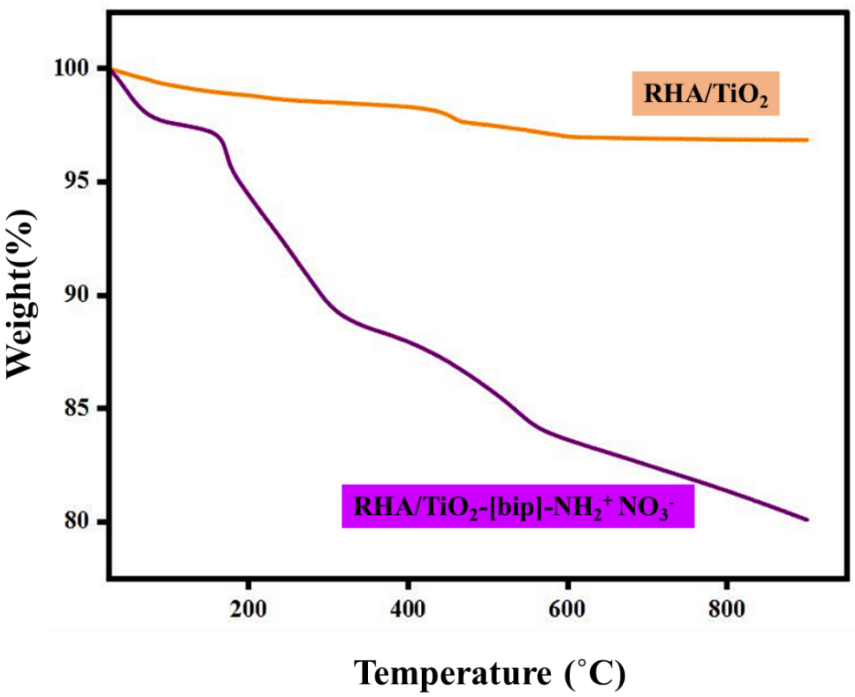

Fig. 4. TGA curve of RHA/TiO_2 and RHA/TiO_2-[bip]-NH_2^+ NO_3^-.

The energy-dispersive X-ray spectroscopy (EDX) of the prepared catalyst shows the presence of oxygen (O), silicon (Si), titanium (Ti), carbon (C), nitrogen (N), potassium (K), phosphorus (P), magnesium (Mg), and iron (Fe) atoms in the pure catalyst's composition (Fig. 5), It should be mentioned that K, P, Mg and Fe are the elements are present in RHA. with the quantitative results from EDX detailed in Table 1.

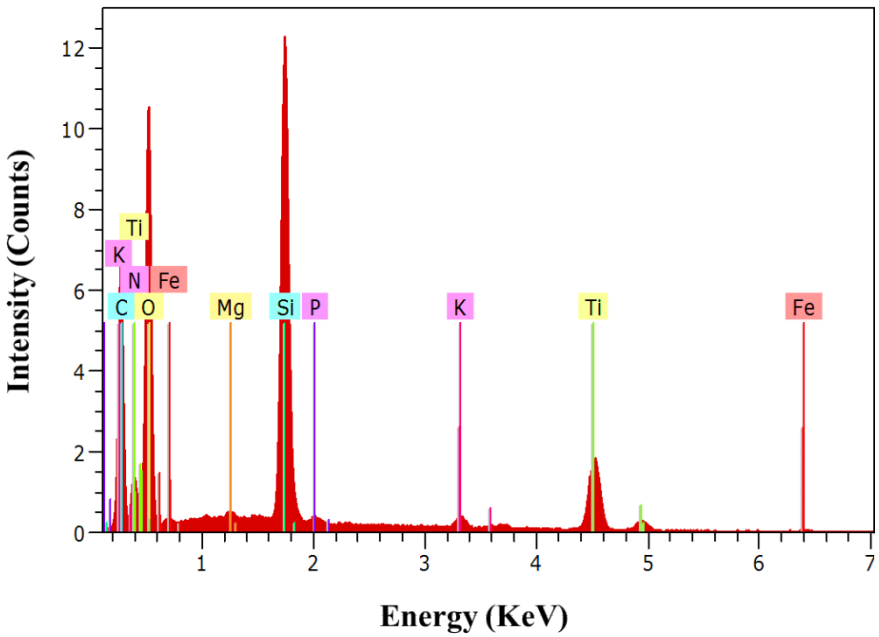

Fig. 5. The EDX profiles of RHA/TiO_2-[bip]-NH_2^+ NO_3^-.

Table 1

Weight percentage of various elements obtained from EDX.

Element	Line	Mass%	Atom%
C	K	22.24	34.89
N	K	1.87	2.51
O	K	35.19	41.44
Mg	K	0.15	0.12
Si	K	18.12	12.16
P	K	0.23	0.14
K	K	0.99	0.48
Ti	K	19.79	7.79
Fe	K	1.42	0.48
Total		100.00	100.00

The XPS survey for RHA/TiO_2-[bip]-NH_2^+ NO_3^- identified species such as Ti 2p, Si 2p, N 1s, and C 1s (Fig. 6a). The Ti 2p spectrum showed peaks at 458.38 and 463.98 eV,

corresponding to Ti^{+4} $2p_{3/2}$ and $2p_{1/2}$ (Fig. 6b) [49,50]. Additionally, peaks related to Si-OH/Si-O-Ti/Si-C, Si-O-Si, and SiO_2 appeared at 102.18, 102.28, and 102.88 eV, respectively (Fig. 6c) [51,52]. The N 1s spectra displayed peaks for C-N, NH_2^+, and NO_3^-, with C-N and NH_2^+ peaks at 399.08 and 401.58 eV, while the NO_3^- peak was at 406.58 eV (Fig. 6d) [53,54]. Peaks at 284.58, 285.68, and 286.48 eV were assigned to C-C, C-N, and C-Si-O forms of C 1s (Fig. 6e) [55,56].

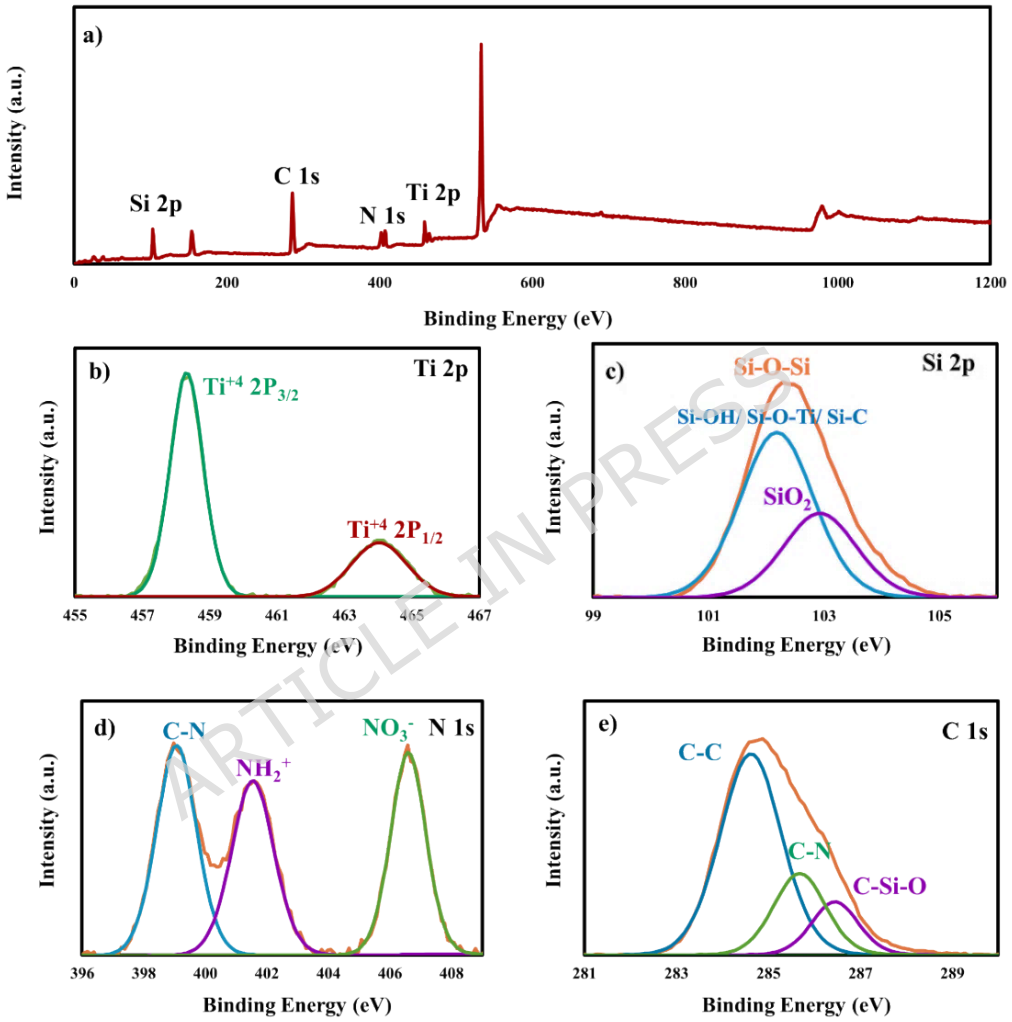

Fig. 6. XPS analysis of RHA/TiO_2-[bip]-NH_2^+ NO_3^- corresponding to: a) Survay, b) Ti 2p, c) Si 2p, d) N 1s, and e) C 1s.

The samples of RHA/TiO_2, RHA/TiO_2-[bip]-NH, and RHA/TiO_2-[bip]-NH_2^+ NO_3^- were examined using field emission scanning electron microscopy (SEM), (Figs. 7a-7c), and transmission electron microscopy (TEM), (Figs. 7d-7f), to determine the size distribution, particle shape, and surface morphology. SEM images reveal that RHA exhibits a porous and

irregular structure, while TiO_2 particles appear spherical and are well-dispersed within the RHA matrix. SEM and TEM images also show that the initial morphology of RHA/TiO_2 changes after modification with the ionic liquid. In fact, comparing the shapes clearly shows that the particles aggregate after modification. In TEM, dark particles indicate RHA/TiO_2 nanoparticles, and the gray background indicates organic compounds.

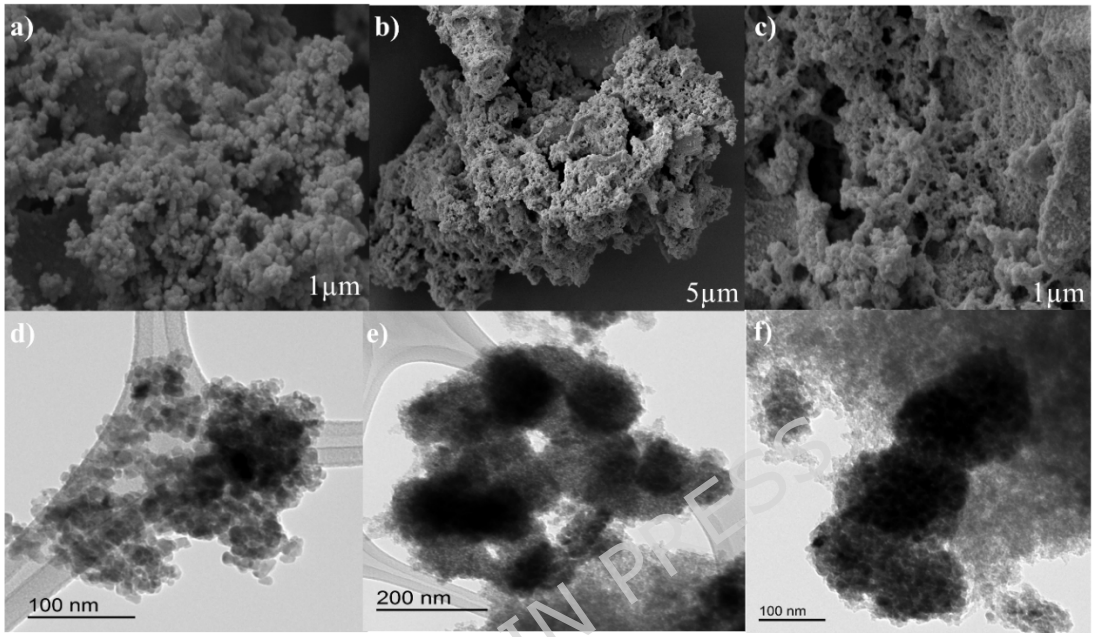

Fig. 7. SEM images of : a) RHA/TiO_2 ,b) RHA/TiO_2-[bip]-NH, and c) RHA/TiO_2-[bip]-NH_2^+ NO_3^- and TEM images of: d) RHA/TiO_2 ,e) RHA/TiO_2-[bip]-NH, and f) RHA/TiO_2-[bip]-NH_2^+ NO_3^-.

Elemental mapping (Fig. 8), confirmed the presence of Si, Ti, C, and N elements in the structure of the RHA/TiO_2-[bip]-NH_2^+ NO_3^- catalyst.

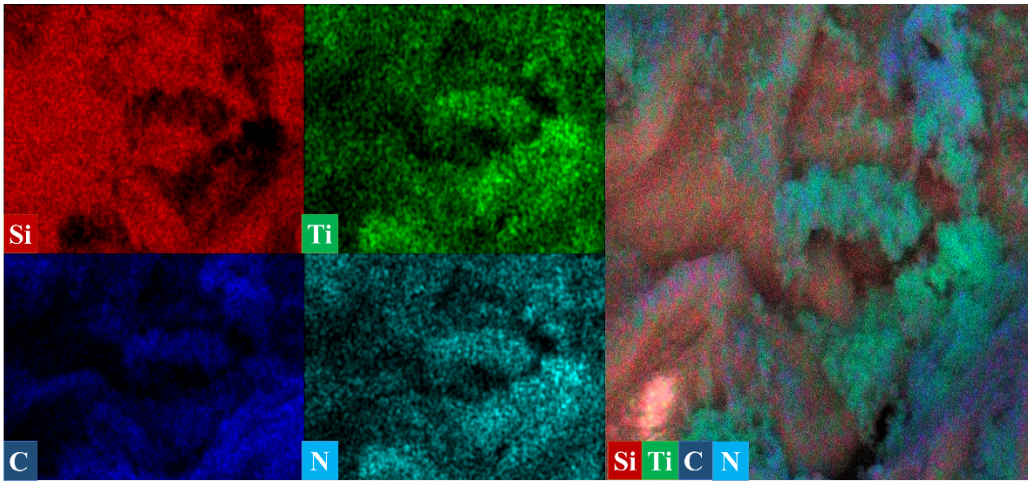

Fig. 8. Corresponding elemental mapping images of the RHA/TiO_2-[bip]-NH_2^+ NO_3^- catalyst.

pH analysis of the catalyst

The acidity of the catalyst was evaluated by monitoring the pH change of an aqueous solution. Briefly, 0.5 g of RHA/TiO_2-[bip]-$NH_2^+NO_3^-$ was added to 25 mL of 1 M NaCl solution with an initial pH of 5.3. The mixture was stirred at room temperature for 2 h, resulting in a pH decrease to 3.9. From this change, the catalyst acidity was calculated to be 0.006 mmol H^+ g^{-1} [44]. Although the measured acidity (0.006 mmol H^+ g^{-1}) is moderate, it is sufficient to efficiently activate carbonyl substrates under solvent-free conditions. Recent studies have shown that excessively strong acidity is not required for multicomponent condensations and may even lead to side reactions or catalyst deactivation [57,58]. In this context, the balanced Brønsted acidity of RHA/TiO_2-[bip]-$NH_2^+NO_3^-$ contributes to its high selectivity and rapid reaction rates.

Catalytic activity

Following the synthesis and characterization of the RHA/TiO_2-[bip]-$NH_2^+NO_3^-$ catalyst, its catalytic activity in the synthesis of 2,3-dihydroquinazolin-4(1*H*)-ones and 1,8-dioxo-decahydroacridine derivatives was studied. To this end, the reaction of 4-chlorobenzaldehyde, isatoic anhydride, and ammonium acetate as a representative reaction of 2,3-dihydroquinazolin-4(1*H*)-ones synthesis, has been selected as a model one (Fig. 9), and the influence of different parameters, including the catalyst amounts, solvent type, temperature, and the reaction time, was studied on it (Table 2). the molar percentage of the catalyst relative to the substrate was calculated based on the acid loading of the catalyst.

The obtained results from these studies revealed that the use of 40 mg of the catalyst without solvent resulted in a separation efficiency higher than 99% in 5 min (Table 2, Entry 1). Reducing the catalyst amounts to 20 mg did not affect the yield, while further reduction to 12 mg caused a drop in the yield to 85% (Table 2, Entries 2 and 3). In addition, the reaction proceeded well in the absence of solvent and at 100 °C in the presence of 20 mg of the catalyst. To investigate the effect of the solvent, the model reaction was studied in the presence of water, ethanol, dichloromethane, acetone, and water/ethanol using 20 mg of the catalyst. The results (Table 2, Entries 6-11) showed that the reaction was carried out with higher efficiency and more favourable performance in the absence of solvent. The superior performance under solvent-free conditions can be attributed to the higher effective concentration of reactants and enhanced interaction between substrates and the acidic sites of the catalyst. In polar solvents, partial solvation of the active sites and dilution of reactants likely reduce catalytic efficiency. Comparison of the catalytic activity of different compounds showed that the synergistic effect between the structural components of the catalyst plays a decisive role; so that RHA/TiO_2-[bip]-$NH_2^+NO_3^-$ showed the highest catalytic activity compared to other compounds (Table 2, Entries 12-15). Also, in the absence of the catalyst, the reaction yield was only 5%, indicating the essential role of the catalyst (Table 2, Entry 16).

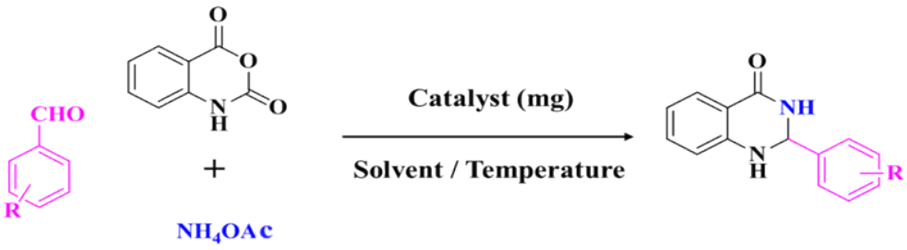

Fig. 9. General reaction for the synthesis of 2,3-dihydroquinazolin-4(1*H*)-ones catalyzed by RHA/TiO_2-[bip]-$NH_2^+NO_3^-$.

Table 2

Optimization of the reaction conditions in the synthesis of 2,3-dihydroquinazolin-4(1*H*)-ones catalyzed by RHA/TiO_2-[bip]-NH_2^+ NO_3^- [a].

Entry	Catalyst	mg of catalyst (mol%)	t (min.)	T(˚C)	Solvent	Yield (%) [b]
1	RHA/TiO_2-[bip]-NH_2^+ NO_3^-	40 (0.024)	5	120	No solvent	>99
2	RHA/TiO_2-[bip]-NH_2^+ NO_3^-	20 (0.012)	5	120	No solvent	>99
3	RHA/TiO_2-[bip]-NH_2^+ NO_3^-	12 (0.007)	60	120	No solvent	85
4	**RHA/TiO_2-[bip]-NH_2^+ NO_3^-**	**20** (0.012)	**5**	**100**	**No solvent**	**>99**
5	RHA/TiO_2-[bip]-NH_2^+ NO_3^-	20 (0.012)	60	80	No solvent	90
6	RHA/TiO_2-[bip]-NH_2^+ NO_3^-	20 (0.012)	180	Reflux	H_2O	43
7	RHA/TiO_2-[bip]-NH_2^+ NO_3^-	20 (0.012)	40	Reflux	EtOH	85
8	RHA/TiO_2-[bip]-NH_2^+ NO_3^-	20 (0.012)	180	Reflux	CH_3CN	15
9	RHA/TiO_2-[bip]-NH_2^+ NO_3^-	20 (0.012)	180	Reflux	CH_2Cl_2	11
10	RHA/TiO_2-[bip]-NH_2^+ NO_3^-	20 (0.012)	180	Reflux	$(CH_3)_2CO$	78
11	RHA/TiO_2-[bip]-NH_2^+ NO_3^-	20 (0.012)	180	70	H_2O/ EtOH	75
12	RHA	20 (-)	120	100	No solvent	60
13	RHA/TiO_2	20 (-)	85	100	No solvent	78
14	RHA/TiO_2-[bip]-NH	20 (0.012)	50	100	No solvent	90
15	HNO_3	20 (-)	60	100	No solvent	42
16	-	-	60	100	No solvent	5

[a] Reaction conditions: 4-chlorobenzaldehyde (1 mmol), isatoic anhydride (1 mmol) and ammonium acetate (1.2 mmol).

[b] Yields are isolated.

With the optimized reaction conditions established, we investigated the reaction between various benzaldehydes, isatoic anhydride, and ammonium acetate (Fig. 10). The results indicated that both types of benzaldehydes containing electron-withdrawing groups and/or electron-donating groups reacted effectively, leading to the formation of the desired products in good to excellent yields (Table 3, Entries 1-14). The turnover number (TON) and turnover frequency (TOF) of the catalyst for the synthesis of 2,3-dihydroquinazolin-4(1H)-one derivatives have been calculated, demonstrating the high efficiency and catalytic activity of the RHA/TiO_2-[bip]-$NH_2^+NO_3^-$ catalyst under the reaction conditions.

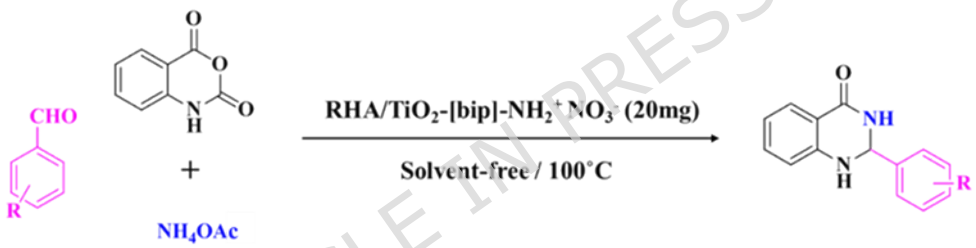

Fig. 10. Model three-component reaction for the synthesis of 2,3-dihydroquinazolin-4(1*H*)-one derivatives.

Table 3

Preparation of 2,3-dihydroquinazolin-4(1*H*)-one derivatives *via* the selected three-component reaction.[a]

				Melting Point

Entry	Substrate	Product	Time (min.)	Yield (%)[b] (TON)[c] (TOF)[d]	Found	Reported [Ref.]
1	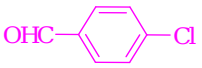	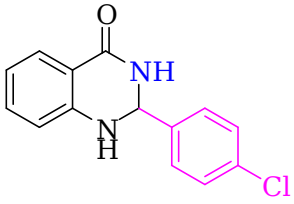	5	99 (8250) (9.9×10^4)	206-208	207-209 [59]
2	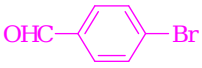	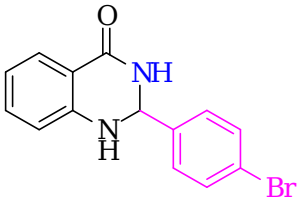	5	99 (8250) (9.9×10^4)	230-232	230-232 [60]
3	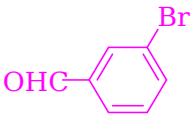	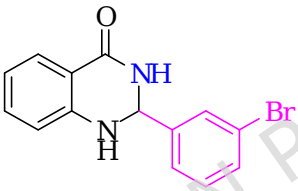	5	99 (8250) (9.9×10^4)	198-200	199-201 [61]
4	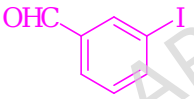	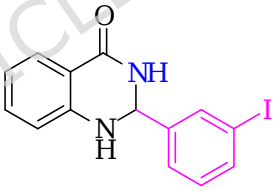	5	99 (8250) (9.9×10^4)	154-155	153-155 [62]
5	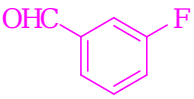	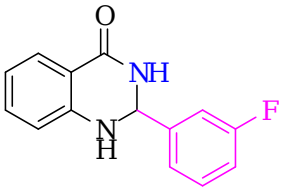	5	99 (8250) (9.9×10^4)	263-264	264-266 [63]

6	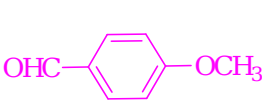	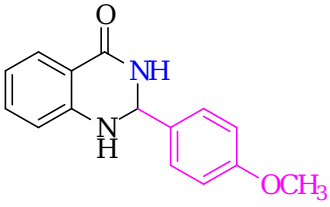	20	97 (8083) (2.4×10^4)	178- 180	178- 180 [64]
7	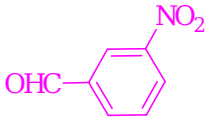	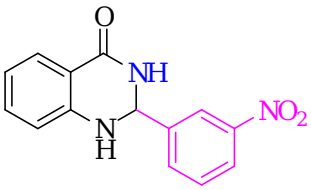	10	98 (8167) (4.9×10^4)	215- 216	216- 218 [65]
8	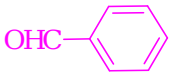	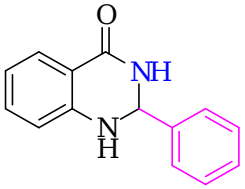	15	95 (7917) (3.2×10^4)	226- 228	226- 227 [66]
9	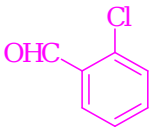	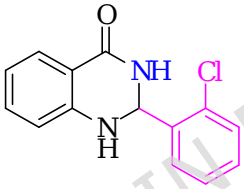	5	94 (7833) (9.4×10^4)	208- 210	210- 211 [67]
10		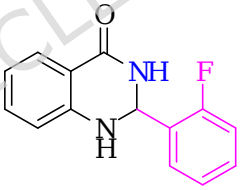	5	93 (7917) (9.3×10^4)	265- 267	265- 267 [68]
11	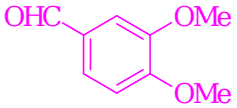	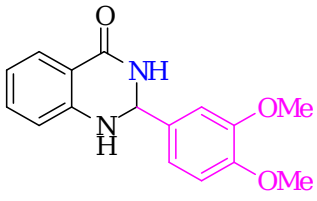	15	90 (7500) (3×10^4)	217- 219	218- 219 [69]
12	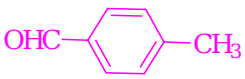	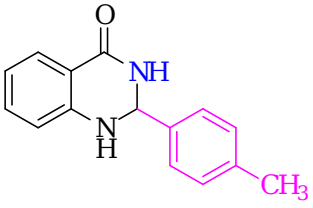	10	89 (7417) (4.4×10^4)	224- 225	222- 224 [70]

13	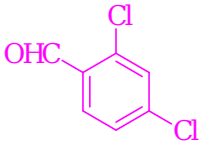	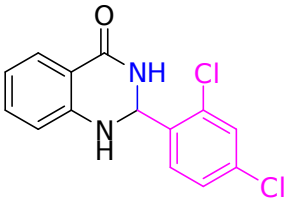	20	91 (7583) (2.3×10^4)	166-168	166-167 [71]
14	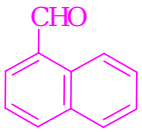	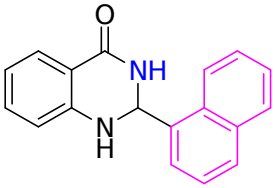	60	88 (7333) (7.3×10^4)	202-205	202-206 [72]

[a] Reaction conditions: aldehyde (1 mmol), isatoic anhydride (1 mmol), and ammonium acetate (1.2 mmol).

[b] Yields are isolated.

[c] TON units (mol of product/mol of catalyst (active sites)).

[d] TOF units (TON/Time(h))

We have proposed in Figure 11 a possible mechanism for the synthesis of 2,3-dihydroquinazolin-4(1*H*)-one derivatives in the presence of the RHA/TiO_2-[bip]-$NH_2^+NO_3^-$ catalyst. According to this mechanism, firstly, the catalyst activates the carbonyl group of isatoic anhydride to facilitate the nucleophilic attack of ammonia on the anhydride group, leading to the formation of 2-aminobenzamide (I) *via* decarboxylation. The activated aldehyde then reacts with 2-aminobenzamide in the presence of the catalyst, eliminating water and forming an imine intermediate (II). The product is then produced *via* intramolecular nucleophilic attack of the amide nitrogen on the imine group.

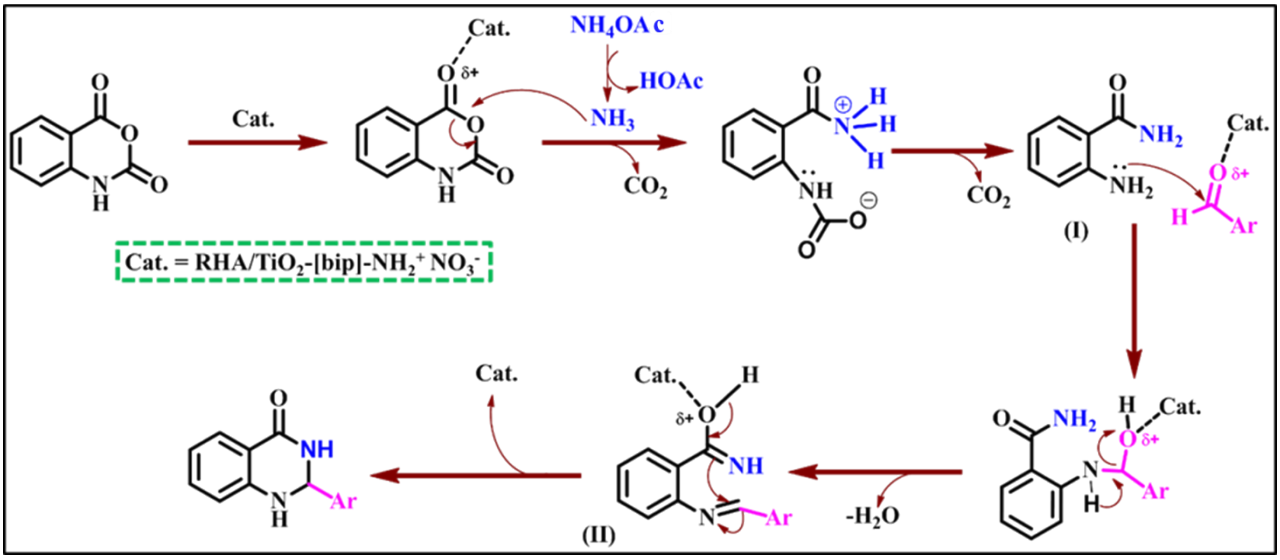

Fig. 11. Plausible mechanism for the synthesis of 2,3-dihydroquinazoline-4-(1*H*)-ones.

The Hammett study for 2,3-dihydroquinazolin-4(1H)-one derivatives was performed to evaluate the electronic effect of substituents on the reaction rate. Only substrates affording high and comparable conversions (≥95% yield) were considered to ensure meaningful comparison. The analysis was restricted to para- and meta-substituted benzaldehydes, while ortho-substituted derivatives were excluded due to steric effects that may deviate from classical Hammett behavior[73] (Table S1). The Hammett plot exhibits a positive slope (ρ = 0.50), indicating a moderate electronic influence, where electron-withdrawing substituents slightly accelerate the reaction (Fig S1). The observed data dispersion suggests that electronic effects are not the sole rate-controlling factor, which is reasonable considering the multistep nature of the reaction and the possible contribution of steric and other non-electronic effects.

A comparison was carried out on the synthesis of 2-(4-chlorophenyl)-2,3-dihydroquinazolin-4(1*H*)-one using the RHA/TiO_2-[bip]-$NH_2^+NO_3^-$ catalyst and several previously reported catalytic systems. The results, which are tabulated in Table 4, demonstrated that the prepared catalyst exhibits superior or at least comparable

performance relative to earlier methods, particularly in terms of reaction time, yield, and overall reaction conditions, thereby highlighting its efficiency.

Table 4

Comparison between the efficiency of some of the catalysts reported in the literature and RHA/TiO_2-[bip]-NH_2^+ NO_3^- in the preparation of 2-(4-chlorophenyl)-2,3-dihydroquinazolin-4(1*H*)-one.

Entry	Catalyst(mg)	Reaction Condition	Time (min.)	Yield (%) [Ref.]	Product
1	$ClCH_2CO_2H$ (20)	EtOH: H_2O (1:4)/60˚C	480	47[74]	
2	$InCl_3$ (10mol%)	Solvent-free/70˚C	120	89[75]	
3	[{SiO_2-(acac)}$_3$Fe (III)] Cl_3 (20)	H_2O/80˚C	60	98[76]	
4	$CoFe_2O_4$@SiO_2@BIMA@Cu (20)	H_2O/Reflux	30	95[77]	
5	$FeCl_3$/neutral Al_2O_3 (100)	*tert*-Butanol/ Reflux	210	88[78]	
6	Lactic acid (18)	Solvent-free/70˚C	30	90[79]	
7	RHA/TiO_2-[bip]-NH_2^+ NO_3^- (20)	Solvent-free/100˚C	5	>99 This work	

After the successful application of RHA/TiO_2-[bip]-$NH_2^+NO_3^-$ as an efficient catalyst in the synthesis of 2,3-dihydroquinazolin-4(1*H*)-one derivatives, we extended its catalytic utility to the synthesis of 1,8-dioxo-decahydroacridine derivatives. The results showed that the synthesis of 1,8-dioxo-decahydroacridine using the previous conditions could be carried out over a long reaction time. To overcome this limitation, the reaction parameters were optimized by increasing both the catalyst loading and the reaction temperature. The most favorable outcome was achieved using 40 mg (0.024 mol%) of RHA/TiO_2-[bip]-$NH_2^+NO_3^-$ at 110 °C (Fig. 12). Under these optimized conditions, a wide range of 1,8-dioxo-decahydroacridine derivatives were synthesized in good to excellent yields, as indicated in Table 5, demonstrating the high catalytic activity and versatility of this system.

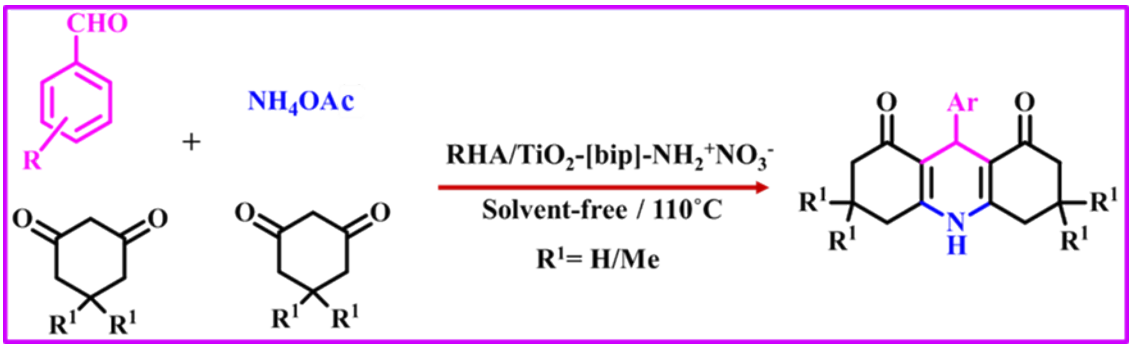

Fig. 12. Synthesis of 1,8-dioxo-decahydroacridine catalysed by RHA/TiO_2-[bip]-$NH_2^+NO_3^-$.

Table 5

Synthesis of various 1,8-dioxo-decahydroacridine derivatives catalysed by RHA/TiO_2-[bip]-$NH_2^+NO_3^-$[a].

Entry	Substrate	R^1	Time (min.)	Product	Yield (%) [b]	Melting Point	
						Found	Reported [Ref.]
1	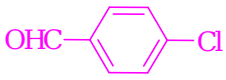	CH_3	10	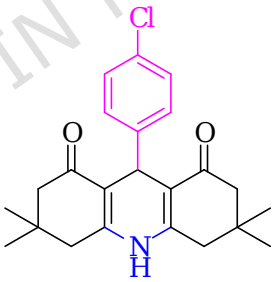	99	294-296	295-297 [80]
2	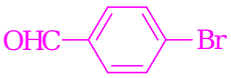	CH_3	10	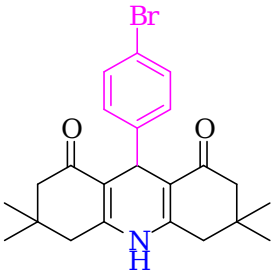	97	314-316	314-316 [81]

3	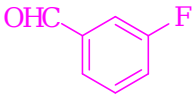	CH_3	10	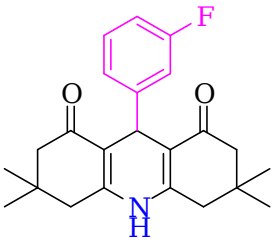	98	300-301	298-300 [82]
4	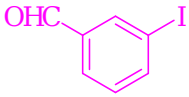	CH_3	10	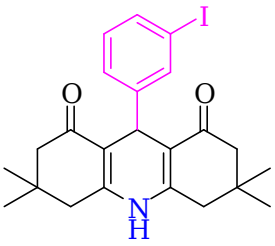	99	313-315	New
5	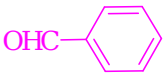	CH_3	10	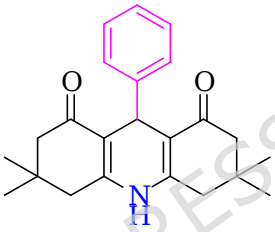	99	278-279	274-276 [83]
6	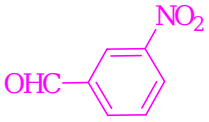	CH_3	10	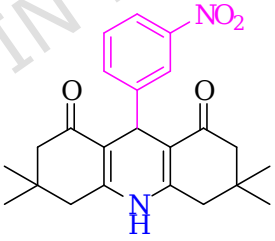	96	298-300	298-300 [84]
7	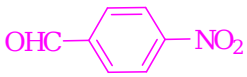	CH_3	10	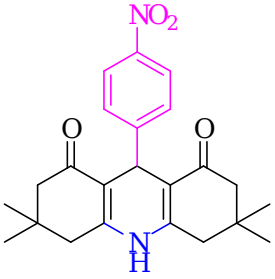	99	266-267	268-270 [85]
8	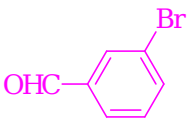	CH_3	10	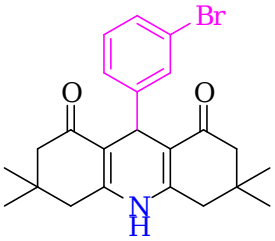	98	287-289	286-288 [86]

9		CH_3	10	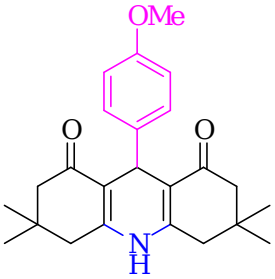	95	301-303	299-300 [87]
10	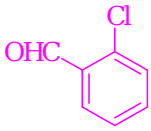	CH_3	10	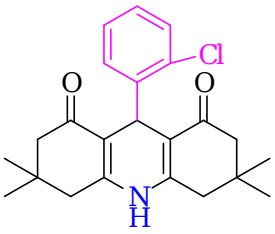	94	287-288	288-290 [88]
11	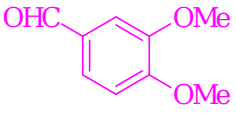	CH_3	10	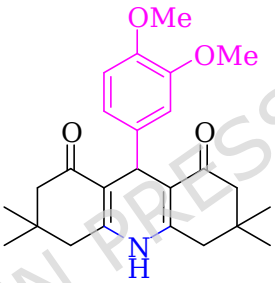	99	275-277	272-274 [89]
12	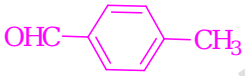	CH_3	10	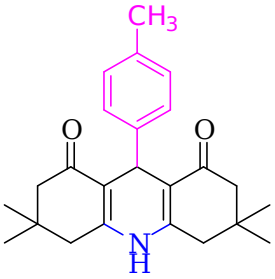	93	263-264	266-268 [90]
13	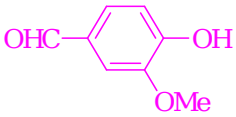	CH_3	15	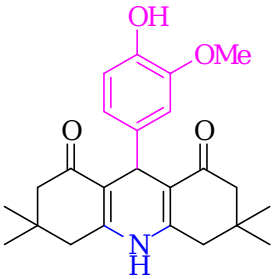	98	294-295	294-295 [91]

14	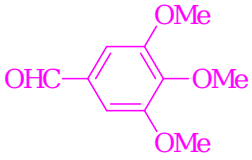	CH_3	10	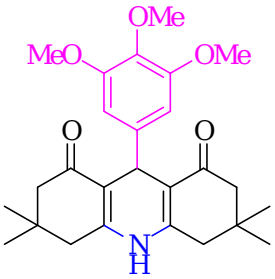	90	245-247	248-250 [92]
15	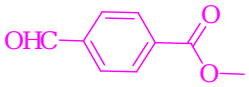	CH_3	10	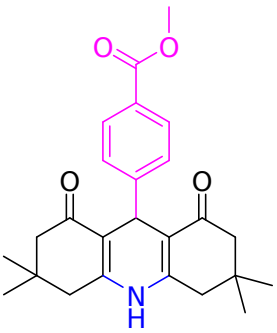	95	232-234	228-230 [93]
16	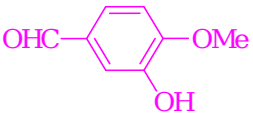	CH_3	15	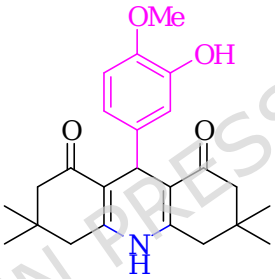	99	299-301	300-304 [94]
17	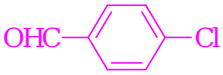	H	10	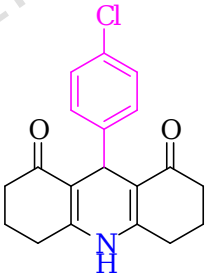	99	292-294	292-294 [95]
18	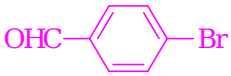	H	10	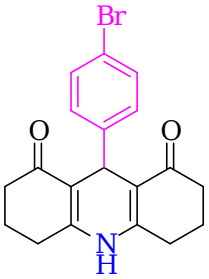	99	313-314	311-312 [96]

19	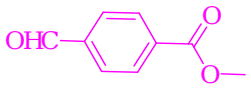	H	10	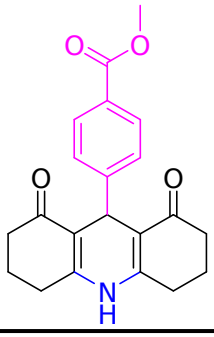	94	233-235	New

[a] Reaction conditions: aldehyde (1 mmol), 1,3-diketones (dimedone or 1,3-cyclohexanedione) (2 mmol), and ammonium acetate (1.5 mmol).
[b] Yields are isolated.

To investigate further the effectiveness of the resulting catalytic system for the preparation of 1,8-dioxodecahydroacridine derivatives, the current protocol was compared with the literature-reported protocols (Table 6). Compared to previously reported catalytic systems, the present catalyst offers a unique combination of mild acidity, heterogeneous nature, and solvent-free operation, which collectively result in significantly reduced reaction times while maintaining excellent yields. Unlike homogeneous acids or metal salts, RHA/TiO_2-[bip]-$NH_2^+NO_3^-$ can be easily recovered and reused without noticeable loss of activity, highlighting its practical and sustainable advantages.

Table 6

Comparison between the efficiency some of the previously reported catalysts and RHA/TiO_2-[bip]-NH_2^+ NO_3^- in the preparation 9-(4-chlorophenyl)-3,3,6,6-tetramethyl-3,4,6,7,9,10-hexahydroacridine-1,8(2*H*,5*H*)-dione.

Entry	Catalyst(mg)	Reaction Condition	Time (min.)	Yield (%) [Ref.]	Product
1	Aluminized Polyborate (20)	Solvent-free/100˚C	25	92[97]	
2	Citric acid (384)	EtOH / Reflux	160	87[98]	

3	Fe^{3+} /4A (20)	EtOH / Reflux	840	99[99]
4	CdS thin film NPs, (1000)	EtOH /80˚C	110	87[100]
5	Sawdust sulfonic acid (50)	EtOH/ Reflux	45	82[101]
6	Fe_3O_4@CS–TDI–Titriplex V (20)	EtOH / Reflux	30	90[102]
7	RHA/TiO_2-[bip]-NH_2^+ NO_3^- (40)	Solvent-free/110˚C	10	99 This work

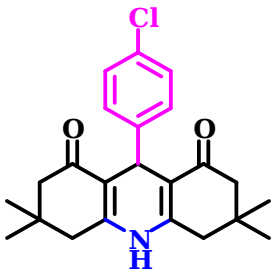

The proposed reaction pathway for synthesizing 1,8-dioxodecahydroacridine derivatives with RHA/TiO_2-[bip]-NH_2^+ NO_3^- is outlined in Figure 13 [103–107]. According to this mechanism, the catalyst functions as a Brønsted acid is the activation of the aldehyde group toward nucleophilic attack. A Knoevenagel condensation between the activated aldehyde and a dimedone generates the intermediate (I). Meanwhile, the reaction of the dimedone with ammonium acetate forms enamine (II). The Knoevenagel adduct (I) then couples with enamine (II) through Michael addition, producing the intermediate (III) (method a). Alternatively (method b), dimedone reacts directly with (I) to form (II), which condenses with ammonium acetate to yield (III). Finally, (III) or its tautomer (III′) undergoes intramolecular attack by the amino group on the carbonyl, followed by dehydration, to afford the target 1,8-dioxodecahydroacridine.

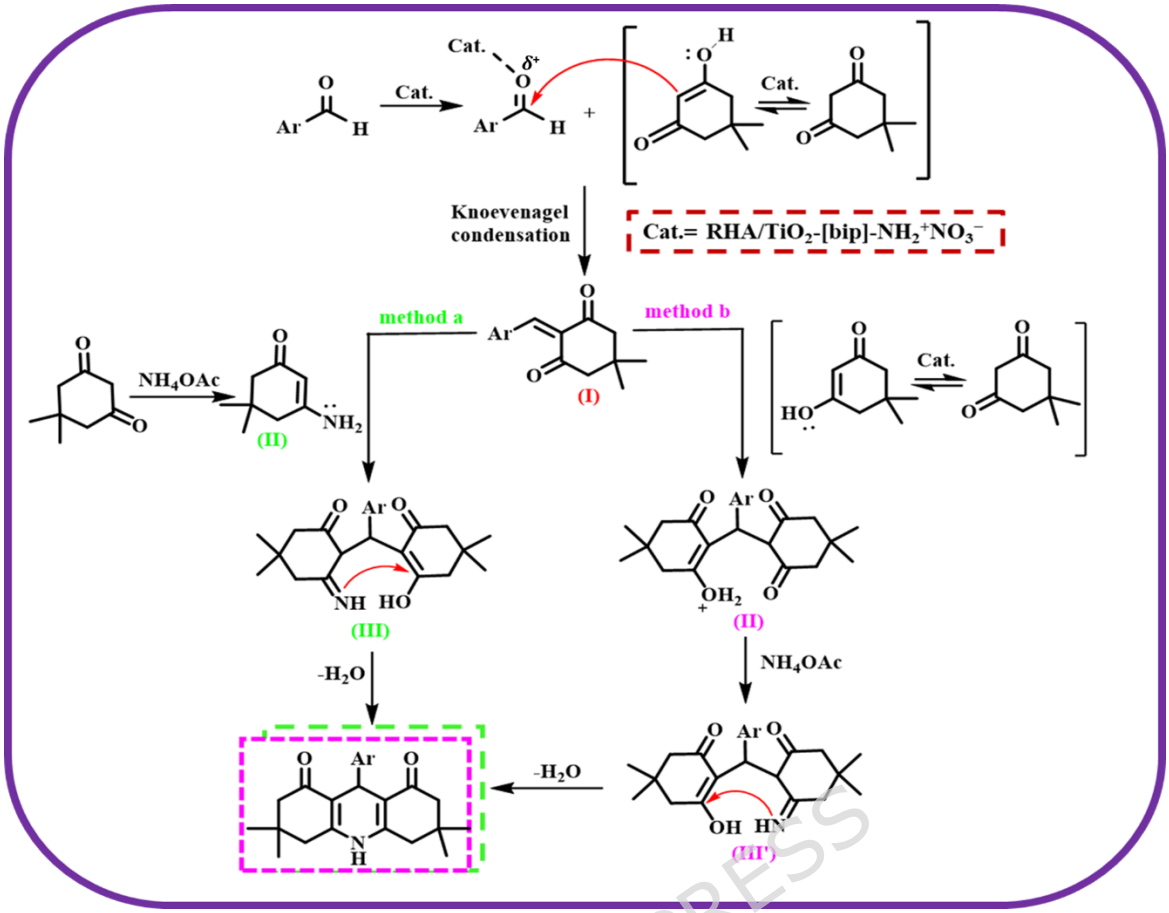

Fig. 13. A Plausible mechanism for the formation of the Hantzsch products in the presence of RHA/TiO_2-[bip]-NH_2^+ NO_3^-.

1. Recycling of the Catalyst

The recyclability of the RHA/TiO_2-[bip]-NH_2^+ NO_3^- catalyst was evaluated to investigate its stability and potential for reuse in two model reactions. In the first reaction, the catalyst was used in the synthesis of 2,3-dihydroquinazolin-4(1*H*)-one derivatives from 4-chlorobenzaldehyde, isatoic anhydride, and ammonium acetate under optimized conditions. In the second reaction, the same catalyst was used to synthesize 1,8-dioxodecahydroacridine derivatives using 4-chlorobenzaldehyde, ammonium acetate, and dimedone under the same optimized conditions. After the reaction was completed, it was dissolved in hot ethanol, and the insoluble catalyst remained, which was separated by filtration, dried at room temperature, and used for the next steps. Then, the recycled

catalyst was reused in the next cycle under the same reaction conditions. Fig. 14 shows that the catalyst could be used for up to five consecutive cycles without any noticeable loss in its catalytic activity. This remarkable recyclability and stability demonstrate the robustness and high efficiency of the catalyst, and demonstrate its compatibility with green chemistry principles.

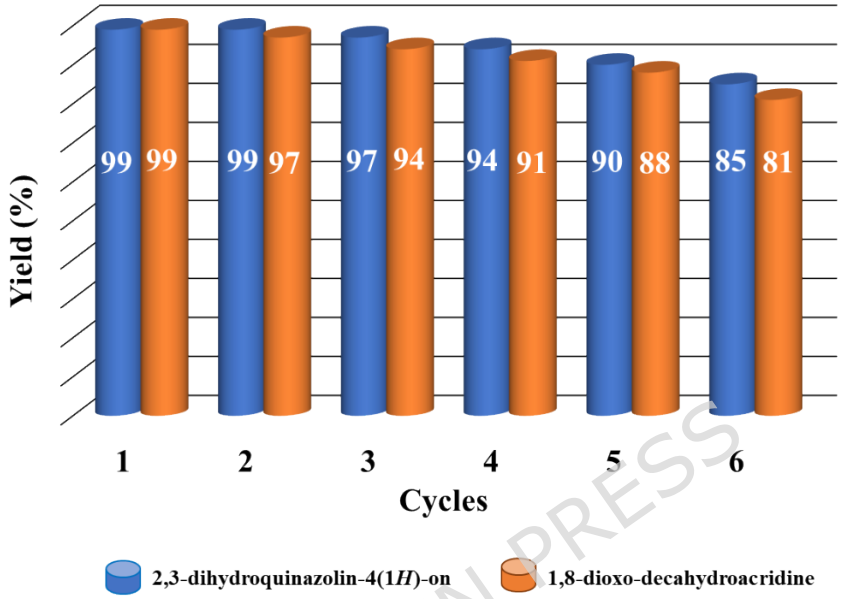

Fig. 14. Reusability of the catalyst.

Furthermore, the XRD pattern of the reused catalyst was almost identical to that of the fresh one, confirming that no significant structural change occurred during the recycling process **(**Fig. 15).

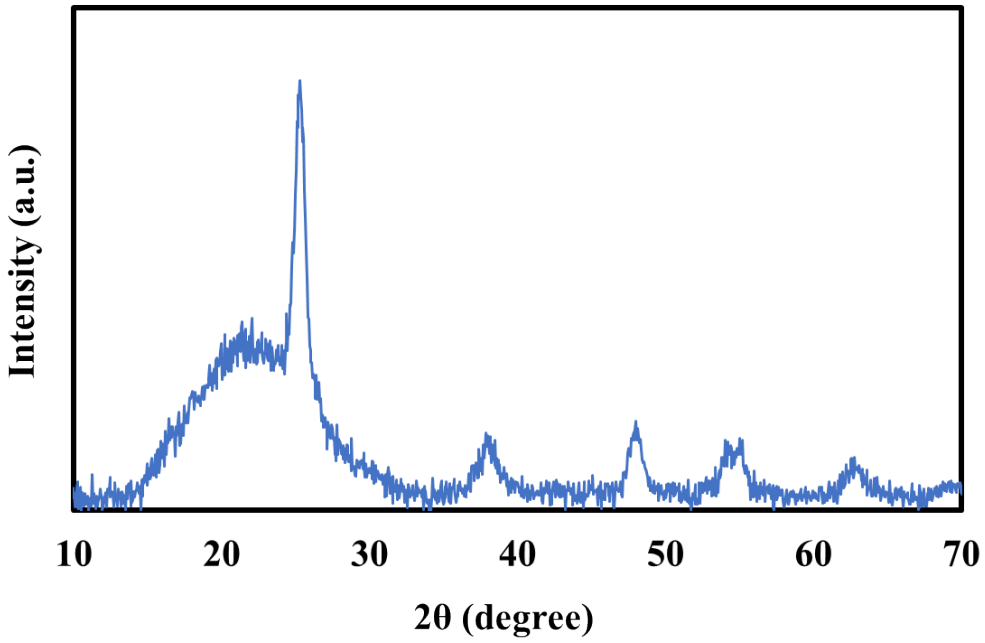

Fig. 15. XRD patterns of the reused catalyst.

Also, the EDX spectrum of the reused catalyst showed the same elemental composition as that of the fresh catalyst, further indicating its stability and retention of key elements (Fig. 16), with the quantitative results from EDX detailed in Table 7.

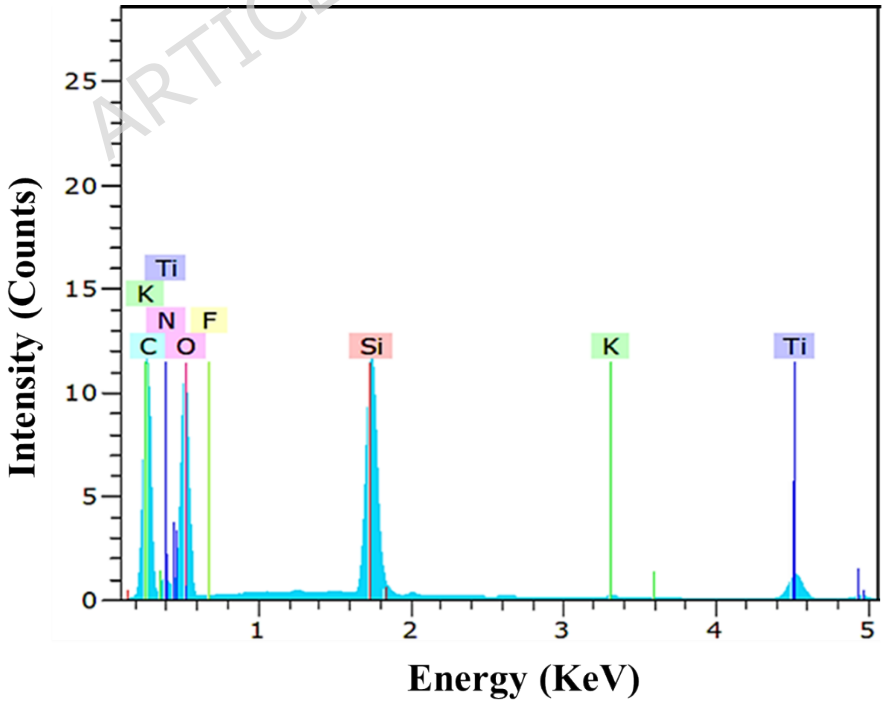

Fig. 16. EDX spectrum of the reused catalyst.

Table 7

Weight percentage of various elements in the recycled catalyst obtained from EDX.

Element	Line	Mass%	Atom%
C	K	34.88	48.10
N	K	2.02	2.39
O	K	33.64	34.83
F	K	0.17	0.14
Si	K	17.96	10.60
K	K	0.28	0.12
Ti	K	11.06	3.83
Total		100.00	100.00

In the XPS analysis, the reused catalyst exhibited a spectral profile consistent with that of the fresh catalyst, indicating its structural stability after multiple reaction cycles (Fig. 17).

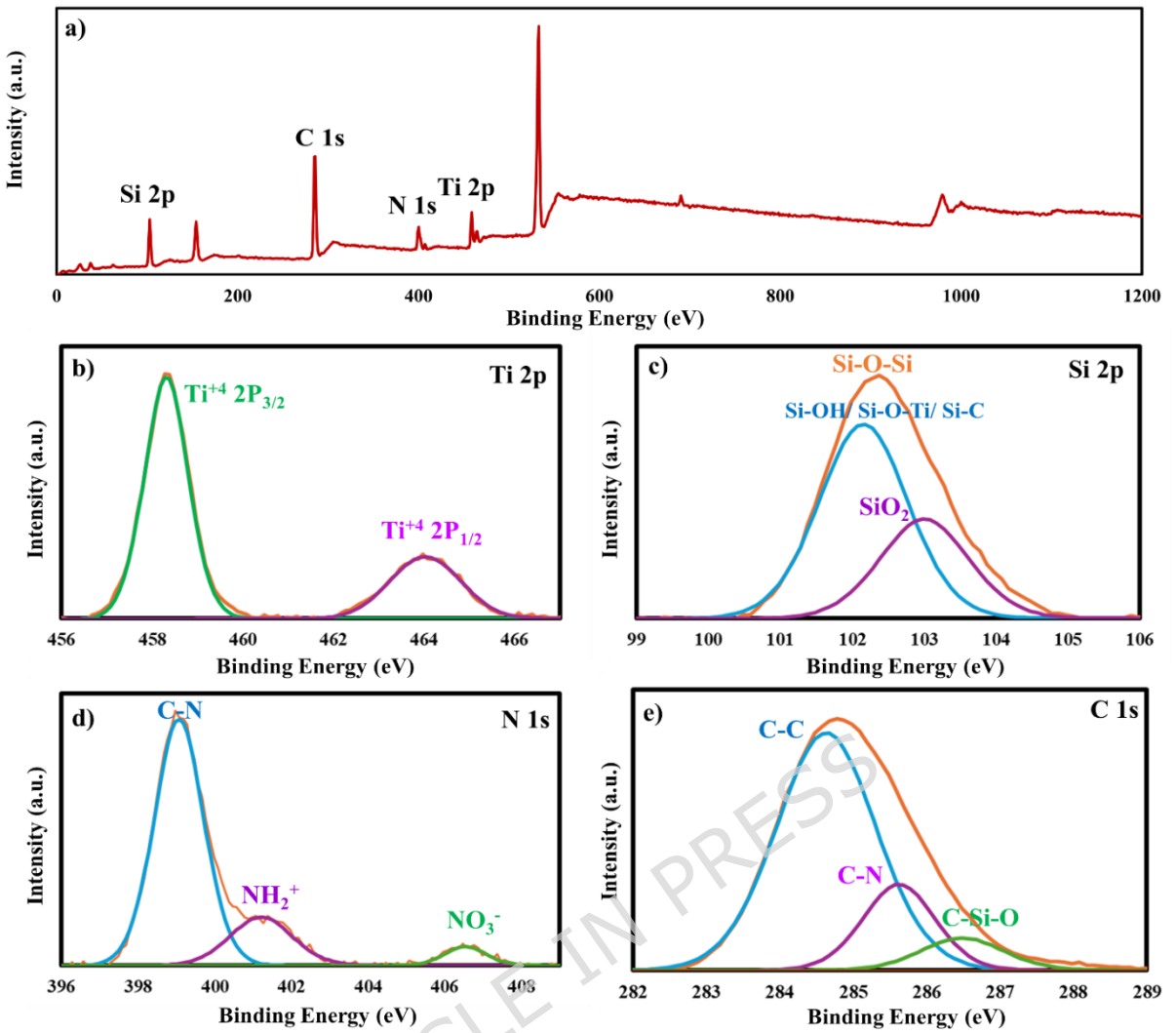

Fig. 17. XPS spectrum of the reused catalyst.

The SEM (Figs. 18a and 18b) and TEM (Figs. 18c and 18d) images of the recycled catalyst were performed to check any change in morphology, and the results exhibited that the catalyst is not significantly affected.

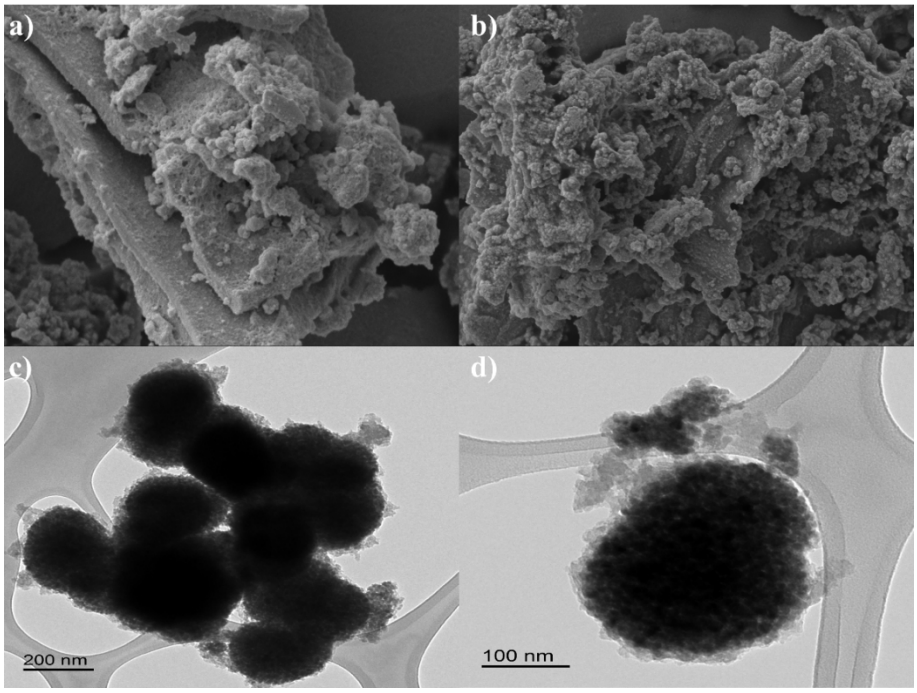

Fig. 18. (a, b) SEM and (c, d) TEM images of the reused catalyst.

After analyzing the elemental mapping (Fig. 19), it was confirmed that all the components present in the fresh catalyst were also detected in the reused one.

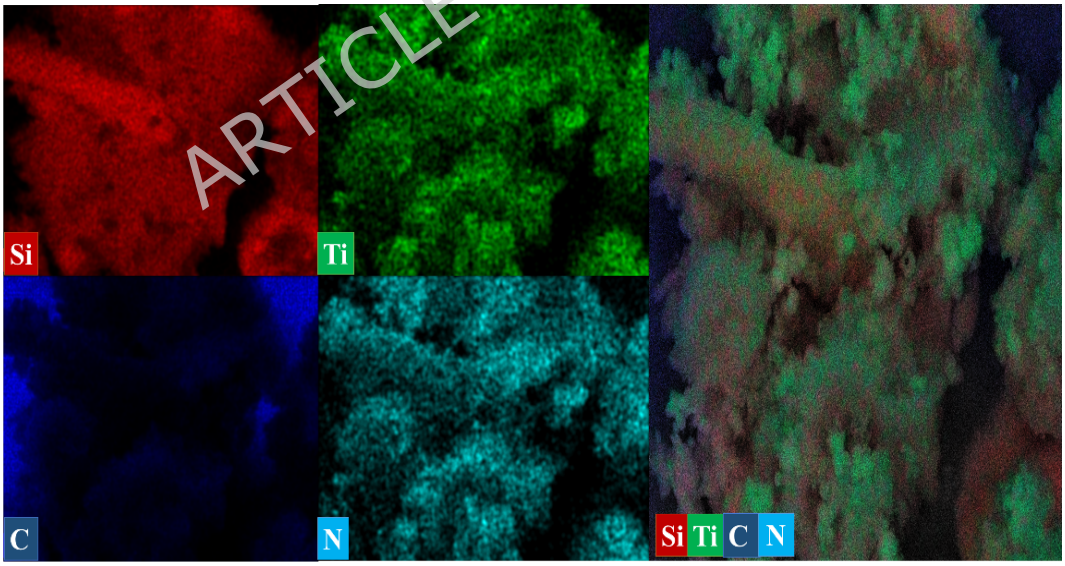

Fig. 19. Corresponding elemental mapping images of the reused catalyst.

The preservation of catalytic activity over five consecutive cycles can be directly correlated with the structural stability of the catalyst. The nearly identical XRD, XPS, SEM, and TEM profiles of the fresh and reused catalysts confirm that no significant structural degradation or leaching of active species occurs during the reaction process. This stability demonstrates the strong immobilization of the ionic liquid moieties on the RHA/TiO_2 surface and explains the excellent recyclability of the catalyst. Such robustness is a key advantage over many reported ionic-liquid-based systems that suffer from gradual deactivation upon reuse.

Conclusion

We thank the reviewer for this valuable suggestion. The conclusion section was rewritten. The RHA/TiO_2-[bip]-$NH_2^+NO_3^-$ catalyst efficiently promoted the solvent-free synthesis of 2,3-dihydroquinazolin-4(1H)-ones (5 min, >99% yield at 100 °C) and 1,8-dioxo-decahydroacridines (10 min, 99% yield at 110 °C). Compared to previous methods, this system exhibited superior reaction times, high yields, greener conditions, and excellent recyclability over five cycles without loss of activity. Comprehensive characterization (FT-IR, XRD, XPS, TGA, SEM, and TEM) confirmed the catalyst's structural stability and effective active sites.

Future work may focus on scale-up applications in industrial multicomponent reactions, deeper mechanistic investigations (e.g., DFT studies), evaluation of biological activities of the products, and catalyst optimization through anion modification or alternative supports.

Acknowledgments

The authors thank the Research Council of the University of Guilan, IASBS, and the University of Alicante for helping to do this work.

Data availability

The data that support the findings of this study are available from the corresponding author upon reasonable request.

Reference

1. Shen, X., Hong, G. & Wang, L. Recent advances in green multi-component reactions for heterocyclic compound construction. *Org. Biomol. Chem.* **23**, 2059–2078 (2025).
2. Tandi, M., Sharma, V., Gopal, B. & Sundriyal, S. Multicomponent reactions (MCRs) yielding medicinally relevant rings: a recent update and chemical space analysis of the scaffolds. *RSC Adv.* **15**, 1447–1489 (2025).
3. Mohlala, R. L., Rashamuse, T. J. & Coyanis, E. M. Highlighting multicomponent reactions as an efficient and facile alternative route in the chemical synthesis of organic-based molecules: a tremendous growth in the past 5 years. *Front. Chem.* **12**, (2024).
4. Zhang, X., Lu, X., Zhang, P., Dai, M. & Liang, T. Recent Advances in the Multicomponent Reactions of Indoles. *European J. Org. Chem.* **28**, e202401446 (2025).
5. Carvalho, M. H. R., de Castro, P. P., de Oliveira, K. T. & Amarante, G. W. Enhancing Efficiency and Sustainability: Unleashing the Potential of Continuous Flow in Multicomponent Reactions. *ChemSusChem* **18**, e202401840 (2025).
6. Ingale, A. A., Kagne, R. P., Ghanwat, V. B., & Sargar, A. M. ZrO_2 as an efficient heterogeneous catalyst for the synthesis of 2-benzylidene malononitrile derivatives via Knoevenagel condensation. *Interactions* **246**, 94 (2025).
7. Ingale, A. A., Kagne, R. P., Topkar, R. R., Kulal, S. R. & Sargar, A. M. $LaCoO_3/Co_3O_4$ catalyzed synthesis of tetrahydro benzo[b]pyran derivatives and their in vitro, in silico anticancer evaluation. *J. Indian Chem. Soc.* **102**, 102230 (2025).

8. Chahar, M. *et al.* Recent advances in the synthesis of nitrogen-containing heterocyclic compounds via multicomponent reaction and their emerging biological applications: a review. *J. Iran. Chem. Soc.* **22**, 1–33 (2025).
9. Liu, J. *et al.* Recent advances in the synthesis of nitrogen heterocycles via Rh(III)-catalyzed chelation-assisted C–H activation/annulation with diazo compounds. *Org. Chem. Front.* **12**, 3065–3106 (2025).
10. Nguyen, H. T., Nguyen, T. T., Doan, V. T. C., Nguyen, T. H. & Tran, M. H. Recent advances in metal-free catalysts for the synthesis of N-heterocyclic frameworks focusing on 5- and 6-membered rings: a review. *RSC Adv.* **15**, 9676–9755 (2025).
11. Ha, H.-J. Recent advances in synthesizing and utilizing nitrogen-containing heterocycles. *Front. Chem.* **11**, (2023).
12. Maity, P. & Mitra, A. K. Ionic liquid-assisted approaches in the synthesis of nitrogen-containing heterocycles: A focus on 3- to 6-membered rings. *J. Ion. Liq* **5**, 100146 (2025).
13. Wong, X. K. & Yeong, K. Y. A Patent Review on the Current Developments of Benzoxazoles in Drug Discovery. *ChemMedChem* **16**, 3237–3262 (2021).
14. Faizan, M. *et al.* Hantzsch reaction: The important key for pyridine/dihydropyridine synthesis. *Synth. Commun.* **54**, 1221–1244 (2024).
15. Lavanya, G. *et al.* Recent Advances in the Synthesis of Dihydropyridine and Their Corresponding Fused Systems via Multi-Component Hantzsch Reaction Using Catalytic Nanomaterials. *ChemistrySelect* **9**, e202403664 (2024).
16. Alvim, H. G. O., Júnior, E. N. da S. & Neto, B. A. D. What do we know about multicomponent reactions? Mechanisms and trends for the Biginelli, Hantzsch, Mannich, Passerini and Ugi MCRs. *RSC Adv.* **4**, 54282–54299 (2014).
17. Liu, G., Pan, R., Wei, Y. & Tao, L. The Hantzsch Reaction in Polymer Chemistry: From Synthetic Methods to Applications. *Macromolecular Rapid Commun.* **42**, 2000459 (2021).

18. Badolato, M., Aiello, F. & Neamati, N. 2,3-Dihydroquinazolin-4(1H)-one as a privileged scaffold in drug design. *RSC Adv.* **8**, 20894–20921 (2018).
19. Zhang, X., Pang, Q., Liu, D. & Zhang, G. Selective synthesis of 2,3-dihydroquinazolin-4(1*H*)-ones and their *N*1-substituted analogues via Pd(II)-catalyzed cascade annulation of *o*-aminobenzoic acids with CO, ammonium acetate and aldehydes. *Tetrahedron* **155**, 133915 (2024).
20. Rijwan, Kumar, S. & Kumar, S. Green and sustainable approaches in the synthesis of pharmaceutically relevant quinazolinones. *Tetrahedron* **172**, 134437 (2025).
21. Deng, Z. *et al.* Quinazolinones as Potential Anticancer Agents: Synthesis and Action Mechanisms. *Biomolecules* **15**, 210 (2025).
22. Pele, R. *et al.* Antioxidant and Cytotoxic Activity of New Polyphenolic Derivatives of Quinazolin-4(3H)-one: Synthesis and In Vitro Activities Evaluation. *Pharmaceutics* **15**, 136 (2022).
23. Amarasekara, A. S. Acidic Ionic Liquids. *Chem. Rev.* **116**, 6133–6183 (2016).
24. Sarkar, A. & Pandey, S. Applications of Ionic Liquids in Green Catalysis: A Review of Recent Efforts. *Curr. Catal.* **10**, 165–178.
25. Zhu, M. Ionic-liquid/metal-organic-framework composites: synthesis and emerging sustainable applications. *Inorg. Chem. Front.* **12**, 39–84 (2025).
26. Wang, P. & Wang, R. Ionic Liquid-Catalyzed CO_2 Conversion for Valuable Chemicals. *Molecules* **29**, 3805 (2024).
27. Qi, Z. *et al.* Challenges and perspectives on using acidic ionic liquids for biodiesel production via reactive distillation. *Green Chem.* **26**, 7718–7731 (2024).
28. Salas, R. *et al.* Ionic liquids in polymer technology. *Green Chem.* **27**, 1620–1651 (2025).
29. Zhang, Q. *et al.* Recent advances in supported acid/base ionic liquids as catalysts for biodiesel production. *Front Chem* **10**, 999607 (2022).

30. Lu, Q. *et al.* MCM-41 supported quaternary ammonium ionic liquids as an effective heterogeneous catalyst for CO_2 cycloaddition reaction. *J Porous Mater* **31**, 897–912 (2024).

31. Tavera-Méndez, C.-L. *et al.* Self-Assembled Supported Ionic Liquids. *Chem. - Eur. J.* **30**, e202303673 (2024).

32. Ingale, A. A., Kagne, R. P. & Sargar, A. M. $NiFe_2O_4$@PPA-DABCO: A novel magnetically separable bifunctional nanocatalyst for the synthesis of 2,2´-(Arylmethylene) bis(3-hydroxy-5,5-dimethyl-2-cyclohexene-1-one) derivatives. *J Nanopart Res* **27**, 77 (2025).

33. Mazloumi, M. & Shirini, F. Nano Rice Husk Ash Modified with Acidic Ionic Liquid Bridge: An Efficient Promoter for the Synthesis of 1,2,4-Triazolo Quinazolinones. *Poly. Arom. Comp.* **43**, 8171–8185 (2023).

34. Mazloumi, M., Shirini, F., Goli-Jolodar, O. & Seddighi, M. Nanoporous TiO_2 containing an ionic liquid bridge as an efficient and reusable catalyst for the synthesis of N, N′-diarylformamidines, benzoxazoles, benzothiazoles and benzimidazoles. *New J. Chem.* **42**, 5742–5752 (2018).

35. Vesoloski, J. F. *et al.* Immobilization of Lipase from Candida antarctica B (CALB) by Sol-Gel Technique Using Rice Husk Ash as Silica Source and Ionic Liquid as Additive. *Appl. Biochem. Biotechnol.* **194**, 6270–6286 (2022).

36. Nasir, I. *et al.* A review of rice husk silica as a heterogeneous catalyst support. *J. Met., Mater. Miner.* **31**, 1–12 (2021).

37. Zhao, Z., Jin, X., Liang, Y., Wang, L.-M. & Liu, Y. D. TiO_2 Nanoparticles Dual-Modified with Ionic Liquid and Acetic Acid for Use as Electrorheological Materials to Achieve Ultrahigh and Stable Electroresponsive Performances. *ACS Appl. Nano Mater.* **5**, 17928–17938 (2022).

38. Balasubramanian, S. *et al.* An Overview of Solid Acid Catalysts in Lignocellulose Biorefineries. *Catalysts* **15**, 432 (2025).

39. Ansari, M. *et al.* Heterogeneous solid acid catalysts for sustainable biodiesel production from wastewater-derived sludge: A systematic and critical review. *Chem. Eng. J. Adv.* **22**, 100718 (2025).

40. Shirini, F., Akbari-Dadamahaleh, S. & Mohammad-Khah, A. Rice husk ash supported $FeCl_2{\cdot}2H_2O$: A mild and highly efficient heterogeneous catalyst for the synthesis of polysubstituted quinolines by Friedländer heteroannulation. *Chinese J. Catal.* **34**, 2200–2208 (2013).

41. An, D., Guo, Y., Zhu, Y. & Wang, Z. A green route to preparation of silica powders with rice husk ash and waste gas. *Chem. Eng. J.* **162**, 509–514 (2010).

42. Shirini, F., Akbari-Dadamahaleh, S. & Mohammad-Khah, A. Rice husk ash supported $FeCl_2{\cdot}2H_2O$: A mild and highly efficient heterogeneous catalyst for the synthesis of polysubstituted quinolines by Friedländer heteroannulation. *Chinese J. Catal.* **34**, 2200–2208 (2013).

43. Shirini, F., Akbari-Dadamahaleh, S., Mohammad-Khah, A. & Aliakbar, A.-R. Rice husk: A mild, efficient, green and recyclable catalyst for the synthesis of 12-Aryl-8, 9, 10, 12-tetrahydro [a] xanthene-11-ones and quinoxaline derivatives. *C. R. Chim.* **16**, 207–216 (2013).

44. Seddighi, M., Shirini, F. & Mamaghani, M. Brønsted acidic ionic liquid supported on rice husk ash (RHA-[pmim]HSO_4): A highly efficient and reusable catalyst for the synthesis of 1-(benzothiazolylamino)phenylmethyl-2-naphthols. *C. R. Chim.* **18**, 573–580 (2015).

45. Seddighi, M., Shirini, F. & Goli-Jolodar, O. Preparation, characterization and application of RHA/TiO_2 nanocomposites in the acetylation of alcohols, phenols and amines. *C. R. Chim.* **19**, 1003–1010 (2016).

46. Abdolmohammad-Zadeh, H., Tavarid, K. & Talleb, Z. Determination of Iodate in Food, Environmental, and Biological Samples after Solid-Phase Extraction with Ni-Al-Zr Ternary Layered Double Hydroxide as a Nanosorbent. *Sci. World J.* **2012**, 145482 (2012).

47. Joao, K. Thermo-Gravimetric Analysis in the Investigation of Catalysts: Insights and Innovations. *J. Chromatogr. Sep. Tech.***15**, 1–2 (2024).

48. Moseson, D. E. *et al.* Application and limitations of thermogravimetric analysis to delineate the hot melt extrusion chemical stability processing window. *Int. J. Pharm.* **590**, 119916 (2020).

49. Xie, W., Li, R. & Xu, Q. Enhanced photocatalytic activity of Se-doped TiO_2 under visible light irradiation. *Sci. Rep.* **8**, 8752 (2018).

50. Nawaz, R. *et al.* Synthesis of Black-TiO_2 and manganese-doped TiO_2 nanoparticles and their comparative performance evaluation for photocatalytic removal of phenolic compounds from agro-industrial effluent. *J. Nanopart. Res.* **23**, 263 (2021).

51. P. Ferreira-Neto, E. *et al.* Thermally stable SiO_2@TiO_2 core@shell nanoparticles for application in photocatalytic self-cleaning ceramic tiles. *Materials Adv.* **2**, 2085–2096 (2021).

52. Kaur, A., Chahal, P. & Hogan, T. Selective Fabrication of SiC/Si Diodes by Excimer Laser Under Ambient Conditions. *IEEE Electron Device Lett.* **37**, 142–145 (2016).

53. Lara, G. G. *et al.* Protection of normal cells from irradiation bystander effects by silica-flufenamic acid nanoparticles. *J. Mater. Sci.: Mater. Med.* **29**, 130 (2018).

54. Stevens, J. S. *et al.* Proton transfer and hydrogen bonding in the organic solid state: a combined XRD/XPS/ssNMR study of 17 organic acid–base complexes. *Phys. Chem. Chem. Phys.* **16**, 1150–1160 (2013).

55. Gholinejad, M., Aloueian, F. & Sansano, J. M. Nickel–Cobalt Nanoprism Comprising ppm Level of Palladium as an Efficient Catalyst for Sonogashira Reaction. *App. Org. Chem.* **39**, e70180 (2025).

56. Guo, J. *et al.* Atomically thin SiC nanoparticles obtained via ultrasonic treatment to realize enhanced catalytic activity for the oxygen reduction reaction in both alkaline and acidic media. *RSC Adv.* **7**, 22875–22881 (2017).

57. Neto, B. A. D., Rocha, R. O. & Rodrigues, M. O. Catalytic Approaches to Multicomponent Reactions: A Critical Review and Perspectives on the Roles of Catalysis. *Molecules* **27**, 132 (2022).

58. Borah, B. *et al.* Brønsted acid catalyzed mechanochemical domino multicomponent reactions by employing liquid assisted grindstone chemistry. *Sci. Rep.* **13**, 1386 (2023).

59. Mohammad, F., Azizi, N., Mirjafari, Z. & Mokhtari, J. Catalytic acidic deep eutectic mixture for efficient and promising synthesis of quinazolinone and quinoxaline derivatives. *RSC Adv.* **15**, 25971–25984 (2025).

60. Ghosh, T., Mandal, I., Basak, S. J. & Dash, J. Potassium tert-Butoxide Promoted Synthesis of Dihydroquinazolinones. *J. Org. Chem.* **86**, 14695–14704 (2021).

61. Kohli, S., Rathee, G., Hooda, S. & Chandra, R. An efficient approach for the green synthesis of biologically active 2,3-dihydroquinazolin-4(1*H*)-ones using a magnetic EDTA coated copper based nanocomposite. *RSC Adv.* **13**, 1923–1932 (2023).

62. Venugopala, K. N. *et al.* Larvicidal Activities of 2-Aryl-2,3-Dihydroquinazolin -4-ones against Malaria Vector Anopheles arabiensis, In Silico ADMET Prediction and Molecular Target Investigation. *Molecules* **25**, 1316 (2020).

63. Safari, J. & Gandomi-Ravandi, S. Efficient synthesis of 2-aryl-2,3-dihydroquinazolin-4(1*H*)-ones in the presence of nanocomposites under microwave irradiation. *J. Mol. Catal. A: Chem.* **390**, 1–6 (2014).

64. Zhang, X., Pang, Q., Liu, D. & Zhang, G. Selective synthesis of 2,3-dihydroquinazolin-4(1*H*)-ones and their *N*1-substituted analogues via Pd(II)-catalyzed cascade annulation of *o*-aminobenzoic acids with CO, ammonium acetate and aldehydes. *Tetrahedron* **155**, 133915 (2024).

65. Nasirmahale, L. N., Shirini, F. & Jolodar, O. G. Poly(4-vinylpyridinum) trinitromethanide: a useful and efficient heterogeneous catalyst for the synthesis of 2,3-dihydroquinazolin-

4(1*H*)-one derivatives under green conditions. *Res. Chem. Intermed.* **49**, 4383–4403 (2023).

66. Li, Z. A novel magnetic heterojunction NiO@Fe_3O_4 photocatalyst in the synthesis of cardiovascular quinazolin-4(1H)-one drugs. *Chem. Pap.* **79**, 2191–2200 (2025).
67. Jeevananthan, V., Senadi, G. C., Muthu, K., Arumugam, A. & Shanmugan, S. Construction of Indium(III)–Organic Framework Based on a Flexible Cyclotriphosphazene-Derived Hexacarboxylate as a Reusable Green Catalyst for the Synthesis of Bioactive Aza-Heterocycles. *Inorg. Chem.* **63**, 5446–5463 (2024).
68. Dutta, A., Damarla, K., Bordoloi, A., Kumar, A. & Sarma, D. KOH/DMSO: A basic suspension for transition metal-free Tandem synthesis of 2,3-dihydroquinazolin-4(1*H*)-ones. *Tetrahedron Lett.* **60**, 1614–1619 (2019).
69. Rahimi, S. *et al.* Synthesis of antioxidant and antibacterial active quinazolinones by carboxymethyl cellulose@$MnFe_2O_4$ biocatalyst. *Inorg. Chem. Commun.* **158**, 111556 (2023).
70. Kumar, G. *et al.* An eco-friendly, sustainable, and greener approach to the synthesis of Dihydroquinazolin-4(1*H*)-ones using a deep eutectic solvent. *J. Heterocycl. Chem.* **61**, 347–357 (2024).
71. Phulwale, S. P., Waghmare, S. D., Gurav, A. P., Gunturu, K. C., & Hangirgekar, S. P. Biosynthesis of $BiFeO_3$ for $BiFeO_3$@Ag-S-CH_2-COOH as the nanocatalyst for one-pot synthesis of 2, 3-dihydroquinazolin-4(1*H*)-ones and their anti-blood cancer activity. *J. Mol. Struct.* **1338**, 142288 (2025).
72. O'Brien, N. S., Gilbert, J., McCluskey, A. & Sakoff, J. A. 2,3-Dihydroquinazolin-4(1*H*)-ones and quinazolin-4(3H)-ones as broad-spectrum cytotoxic agents and their impact on tubulin polymerisation. *RSC Med. Chem.* **15**, 1686–1708 (2024).
73. Hammett, L. P. The Effect of Structure upon the Reactions of Organic Compounds. Benzene Derivatives. *ACS Publications* https://pubs.acs.org/doi/abs/10.1021/ja01280a022 (2002) doi:10.1021/ja01280a022.

74. Maghsoodlou, M. T. *et al.* Chloroacetic acid-promoted heterocyclic reactions: Efficient preparation of tetrahydropyridines and 2,3-dihydroquinazolin-4(1*H*)-ones. *Iran. J. Catal.* **5**, (2015).

75. Sahu, A., Mishra, S., Sahu, P., Gajbhiye, A. & Agrawal, R. K. Indium(III) Chloride: An Efficient Catalyst for One-Pot Multicomponent Synthesis of 2,3-dihydroquinazoline-4(1*H*)-ones. *Curr. Organocatal.* **5**, 137–144 (2018).

76. Dutta, A. *et al.* Sustainable parts-per-million level catalysis with FeIII: One-pot cascade synthesis of 2,3-dihydroquinazolin-4(1*H*)-ones in water. *App. Org. Chem* **35**, e6116 (2021).

77. Bodaghifard, M. A. & Safari, S. Cu(II) complex-decorated hybrid nanomaterial: a retrievable catalyst for green synthesis of 2,3-dihydroquinazolin-4(1*H*)-ones. *J. Coord. Chem.* **74**, 1613-1627 (2021).

78. Wu, S. J., Zhao, Z. Q., Gao, J. S., Chen, B. H. & Chen, G. F. Efficient one-pot synthesis of 2,3-dihydroquinazoline-4(1*H*)-ones promoted by $FeCl_3$/neutral Al_2O_3. *Res. Chem. Intermed.* **45**, 2327–2339 (2019).

79. Zhaleh, S., Hazeri, N. & Maghsoodlou, M. T. Green protocol for synthesis of 2,3-dihydroquinazolin-4(1*H*)-ones: lactic acid as catalyst under solvent-free condition. *Res. Chem. Intermed.* **42**, 6381–6390 (2016).

80. Karami, Z. & Khodaei, M. M. Preparation, characterization, and application of supported phosphate acid on the UiO-66-NH_2 as an efficient and bifunctional catalyst for the synthesis of acridines. *Res. Chem. Intermed.* **49**, 1545–1561 (2023).

81. Amiri, Z., Malmir, M., Hosseinnejad, T., Kafshdarzadeh, K. & Heravi, M. M. Combined experimental and computational study on Ag-NPs immobilized on rod-like hydroxyapatite for promoting Hantzsch reaction. *J. Mol. Catal.* **524**, 112319 (2022).

82. Heravi, M. M., Hosseinnejad, T. & Nazari, N. Computational investigations on structural and electronic properties of CuI nanoparticles immobilized on modified poly (styrene-co-

maleic anhydride), leading to an unexpected but efficient catalyzed synthesis of 1,4-dihydropyridine via Hantzsch pyridine synthesis. *Can. J. Chem.* ***95****, 530-536* (2017).

83. Li, W., Ma, R., Wang, Z. & Lü, C. Insights for photochemical mechanisms of acridine-1,8-diones: An experimental and theoretical analysis and first application for fluorescence detection of 2,4,6-trinitrophenol. *J. Mol. Liq.* **415**, 126401 (2024).
84. Zhu, A., Liu, R., Du, C., & Li, L. Betainium-based ionic liquids catalyzed multicomponent Hantzsch reactions for the efficient synthesis of acridinediones. *RSC Adv.* **7**, 6679–6684 (2017).
85. Zhu, A., Liu, R., Du, C., & Li, L. Betainium-based ionic liquids catalyzed multicomponent Hantzsch reactions for the efficient synthesis of acridinediones. *RSC Adv.* **7**, 6679–6684 (2017).
86. Alponti, L. H. R., Picinini, M., Urquieta-Gonzalez, E. A. & Corrêa, A. G. USY-zeolite catalyzed synthesis of 1,4-dihydropyridines under microwave irradiation: structure and recycling of the catalyst. *J. Mol. Struct.* **1227**, 129430 (2021).
87. Sheikhveisi, M., Hazeri, N., Lashkari, M., Faroughi Niya, H., & Fatahpour, M. Application of Fe_3O_4@THAM-CH_2CH_2-SCH_2CO_2H Magnetic Nanoparticles as an Acidic, Recyclable and Green Catalyst for the Synthesis of Hexahydroacridine-1,8-diones, Hexahydroquinolines, and 2-Amino-3-cyanopyridines. *Org. Prep. Proced. Int.* **57**, 322–334 (2025).
88. Wang, F.-M., Zhou, L., Li, J.-F., Bao, D. & Chen, L.-Z. Synthesis, Structure, and Biological Activities of 10-Substituted 3,3,6,6-Tetramethyl-9-Aryl-3,4, 6,7,9,10-hexahydroacridine-1,8(2H,5H)-dione Derivatives. *J. Heterocyc. Chem.* **54**, 3120–3125 (2017).
89. Zolfigol, M. A., Karimi, F., Yarie, M. & Torabi, M. Catalytic application of sulfonic acid-functionalized titana-coated magnetic nanoparticles for the preparation of 1,8-dioxodecahydroacridines and 2,4,6-triarylpyridines via anomeric-based oxidation. *App. Org. Chem.* **32**, e4063 (2018).

90. Amiri, Z., Malmir, M., Hosseinnejad, T., Kafshdarzadeh, K. & Heravi, M. M. Combined experimental and computational study on Ag-NPs immobilized on rod-like hydroxyapatite for promoting Hantzsch reaction. *Mol. Catal.* **524**, 112319 (2022).
91. Fan, X., Li, Y., Zhang, X., Qu, G. & Wang, J. An efficient and green preparation of 9-arylacridine-1,8-dione derivatives. *Heteroat. Chem.* **18**, 786–790 (2007).
92. Dhane, N. S. *et al.* Synthesis of 1, 8-dioxodecahydroacridines via Hantzsch condensation using theophylline in an aqueous medium: an eco-friendly and bio-based approach. *Res. Chem. Intermed.* **50**, 1147–1160 (2024).
93. Koteeswari, R., Ashokkumar, P., Malar, E. J. P., Ramakrishnan, V. T. & Ramamurthy, P. Highly selective, sensitive and quantitative detection of Hg^{2+} in aqueous medium under broad pH range. *Chem. Commun.* **47**, 7695–7697 (2011).
94. Chavan, P. N., Pansare, D. N., & Shelke, R. N. Eco-friendly, ultrasound-assisted, and facile synthesis of one-pot multicomponent reaction of acridine-1,8(2H,5H)-diones in an aqueous solvent. *J. Chin. Chem. Soc.* **66**, 822–828 (2019).
95. Sehout, I., Boulcina, R., Boumoud, B., Boumoud, T. & Debache, A. Solvent-free synthesis of polyhydroquinoline and 1,8-dioxodecahydroacridine derivatives through the Hantzsch reaction catalyzed by a natural organic acid: A green method. *Synth. Commun.* **47**, 1185–1191 (2017).
96. Kiani, M. & Mohammadipour, M. Fe_3O_4@SiO_2–MoO_3H nanoparticles: a magnetically recyclable nanocatalyst system for the synthesis of 1,8-dioxo-decahydroacridine derivatives. *RSC Adv.* **7**, 997–1007 (2017).
97. Aute, D., Parhad, A., Vikhe, V., Uphad, B. & Gadhave, A. Aluminized polyborate catalyzed efficient solvent-free synthesis of 1,8-dioxo-decahydroacridines via hantzsch condensation. *Curr. Chem. Lett.* **13**, 417–424 (2024).
98. Green protocol for the synthesis of 1,8-dioxo-decahydroacridines by Hantzsch condensation using citric acid as organocatalyst on JSTOR. *Curr. Sci.* **116**, 936–942 (2019).

99. Magyar, Á. & Hell, Z. An Efficient One-Pot Four-Component Synthesis of 9-Aryl-Hexahydroacridine-1,8-Dione Derivatives in the Presence of a Molecular Sieves Supported Iron Catalyst. *Catal. Lett.* **149**, 2528–2534 (2019).

100. Lavanya, G. *et al.* The First Recyclable, Nanocrystalline CdS Thin Film Mediated Eco-benign Synthesis Of Hantzsch 1, 4 Dihyropyridines, 1, 8-Dioxodecahydroacridine and Polyhydroquinolines derivatives. *App. Org. Chem.* **33**, e5026 (2019).

101. Karhale, S., Patil, M., Rashinkar, G., & Helavi, V. Green and cost effective protocol for the synthesis of 1,8-dioxo-octahydroxanthenes and 1,8-dioxo-decahydroacridines by using sawdust sulphonic acid. *Res. Chem. Intermed.* **43**, 7073–7086 (2017).

102. Hassanzadeh, N., G. Dekamin, M., & Valiey, E. A supramolecular magnetic and multifunctional Titriplex V-grafted chitosan organocatalyst for the synthesis of acridine-1,8-diones and 2-amino-3-cyano-4 H -pyran derivatives. *Nanoscale Adv.* **7**, 99–123 (2025).

103. Pourdasht, S., Mousapour, M., Shirini, F. & Tajik, H. Introduction of a tropine-based dication ionic liquid catalyst for the synthesis of polyhydroquinoline and 1,8-dioxodecahydroacridine derivatives. *Res. Chem. Intermed.* **48**, 4403–4418 (2022).

104. Mazloumi, M. & Shirini, F. Introduction of a new catalyst containing an ionic liquid bridge on nanoporous Na^+- montmorillonite for the synthesis of hexahydroquinolines and 1,8-dioxo-decahydroacridines via Hantzsch condensation. *J. Mol. Struct.* **1217**, 128326 (2020).

105. Nasirmahale, L. N., Shirini, F., Bayat, Y. & Mazloumi, M. Introduction of TiO_2-[bip]-NH_2^+ $C(NO_2)_3^-$ as an effective nanocatalyst for the Hantzsch reactions. *New J. Chem.* **46**, 23129–23138 (2022).

106. Mousapour, M. & Shirini, F. Piperazinium Nano Silica Sulfonate: An Efficient Catalyst for the Hantzsch Reaction. *ChemistrySelect* **6**, 4247–4255 (2021).

107. Asareh, R., Safaiee, M., Moeinimehr, M., & Yaghoobi, F. Design and synthesis, and experimental-computational analysis of an acetic acid-functionalized zinc

tetrapyridinoporphyrazine catalyst for synthesizing acridine and quinoline derivatives. *Sci. Rep.* **15**, 1–22 (2025).